공학박사 학위논문

Spirobiindane-based poly(arylene ether sulfone)s as electrode-binding ionomers for anion exchange membrane fuel cells

음이온 교환 막 연료전지 전극 바인더로 적용한

스파이로바이인데인 기반 폴리아릴렌에테르설폰

고분자 전해질 연구

2019년 8월

서울대학교 대학원

공과대학 화학생물공학부

최 지 은

Abstract

Spirobiindane-based poly(arylene ether sulfone)s as electrode-binding ionomers for anion exchange membrane fuel cells

Jieun Choi

School of Chemical and Biological Engineering

The Graduate School

Seoul National University

Alkaline anion exchange membrane fuel cell (AEMFC) systems have the advantages of their availability of non-noble metals (Ni, Mn, Co, etc.) due to faster electrode reaction kinetics for the oxygen reduction reaction under alkaline conditions. But now it is difficult to commercialize AEMFCs because no material is available to satisfy performance and durability as much as the electrolyte and electrode binder of the proton exchange membrane fuel cells in existence. And most studies of AEMFCs are focused on electrolyte membranes and catalysts, and there are few studies on electrode binders. Purpose of this study is to develop

highly gas permeable ionomer for alkaline anion exchange membrane fuel cells.

Chapter 1 described electric power generation from fuel cells, type of fuel cells, and requirements of polymer electrolytes for AEMFCs.

In Chapter 2, this part addressed introduction of spirobiindane group to poly(arylene ether sulfone) (PES) to build the structure of polymers with intrinsic microporosity (PIMs). A novel PESs (QOH-SBIs), which have spirobiindane and tetra(quaternary ammonium) hydroxide pendant moieties, were synthesized for anion-conducting binder material in membrane electrode assembly (MEA) of AEMFCs. The time-lag method was used to check the gas permeability of the polymers. The high permeability is due to the micro-pores at the molecular level that is formed by the difference in chain thicknesses between two alternating units, thick spirobiindane group and thin arylene ether sulfone group. The inter-chain spacing and chain conformation were measured with wide angle X-ray diffraction (WAXD) and small angle neutron scattering (SANS), respectively. High gas permeability directly affected the performance of AEMFC. The MEA with spirobiindane-modified PES shows 1.2 times higher maximum power density than that of spirobiindane-free PES. A MEA using QOH60-SBI40 achieved a peak power density of 223 mW cm^{-2} and current density of 280 mA cm^{-2} at 0.6 V.

Chapter 3 represented that spirobiindane-based poly(arylene ether sulfone)s with quaternary ammonium-functionalized alkyloxy side chains were synthesized as alkaline anion exchange membrane fuel cell (AEMFC) electrode binding materials. A series of novel AEMFC electrode binding ionomers with different main- and side- chain structures were prepared. The ionomers were characterized by NMR

spectroscopy and thermogravimetric analysis. Single cell performance tests using the ionomers were also carried out. The ionomer sample with a spirobiindane unit in the polymer backbone and quaternary ammonium-functionalized hexyloxy side chain showed good potential for AEMFC applications. The MEA using this ionomer as a binder achieved a peak power density of 140 mW cm^{-2}, a 1.2 times better single cell performance than the case using the ionomer with biphenyl unit in the polymer backbone.

This approach additionally allowed us to optimize AEMFC performance by efficiently establishing three-phase boundaries while avoiding problems caused by the adjustment of the length/amount of ionic side chains.

Keywords: alkaline anion exchange membrane fuel cell, binder, ionomer, intrinsic microporosity, poly(arylene ether sulfone), spirobiindane

Student Number: 2014-30257

Contents

List of Tables

Chapter 1

Chapter 2

Chapter 3

List of Figures and Schemes

Chapter 1

Chapter 2

Chapter 3

Chapter 1. Introduction

1.1. Electric power generation from fuel cells

Although conventional electricity generation techniques based on fossil fuels and nuclear power have greatly contributed to the development of the human civilization, they are far from being environmentally benign, which necessitates the search for alternatives such as solar energy, wind energy, geothermal energy, bioenergy, and hydropower.[1] In particular, solar and wind energies are regarded as clean and sustainable but feature the disadvantages of locality and intermittency, which makes hydropower a better alternative for the reduction of CO_2 emissions and fossil fuel usage. Among the various alternative energy sources, fuel cells exhibit high efficiency and high power density and are therefore regarded as the most promising sources of power for stationary and mobile applications.[2]

In fuel cells, electricity is generated via the chemical reaction of H_2 with O_2 to form water. Ideally, water produced in fuel cells can be re-used to produce H_2 and O_2 by electrolysis (Figure 1.1), which makes fuel cells well integrable with other energy systems of the hydrogen economy (Figure 1.2).[3]

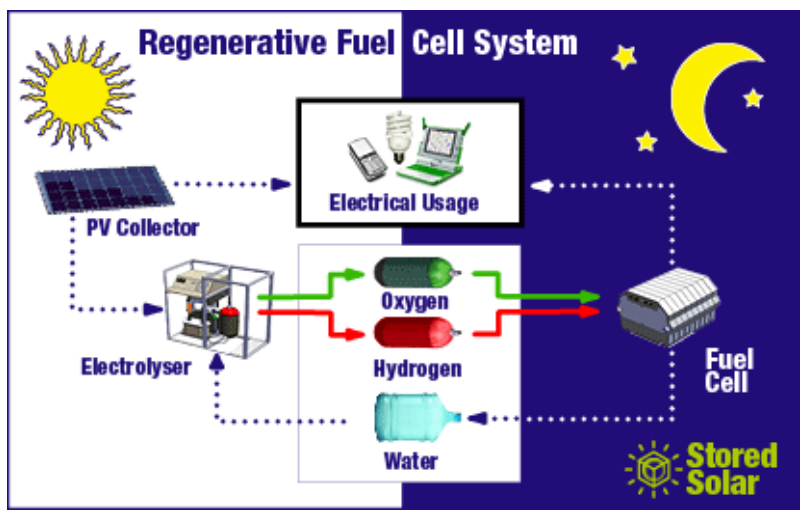

Figure 1.1 Simplified flow diagram of a regenerative fuel cell system using solar power and comprising an electrolyzer and fuel cells. Source: Stored Solar (http://www.storedsolar.com/electrolysers.html).[4]

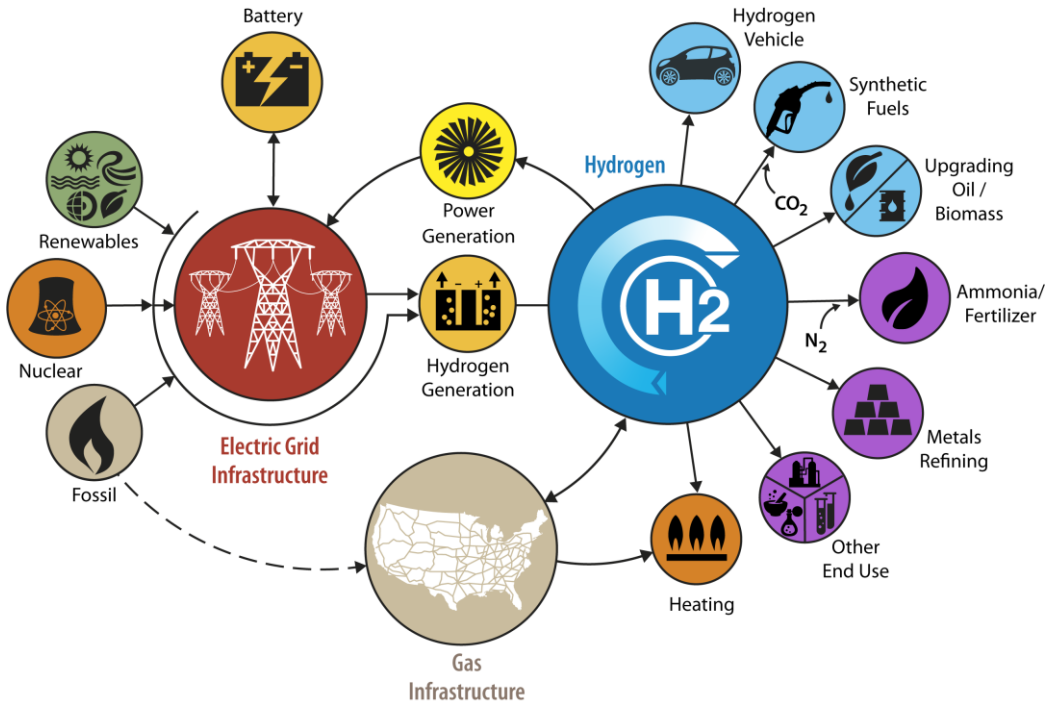

Figure 1.2 Hydrogen as the energy carrier. Source: Energy technologies area, *Hydrogen: the energy carrier of the future. (*https://eta.lbl.gov/news/article/hydrogen-energy-carrier-future).[5]

Fuel cells can be classified according to their electrolyte and operating temperature (Table 1.1), e.g., high-temperature fuel cells are used in power plants, while low-temperature ones are mainly used in the automotive and space industries.[6]

1.2. Polymer electrolyte membrane fuel cells

Polymer electrolyte membrane fuel cells (PEMFCs) use H_2 and O_2 as fuel to form water as the only product, while the potential difference is generated via the transfer of H^+ or OH^- to electrodes through electrolytes (Figure 1.3).[7] The membrane electrode assembly (MEA) is a key component of PEMFCs that determines cell performance and comprises polymer electrolyte and catalyst layers.[8]

Ion-exchange membranes, i.e., polymer electrolytes, are separator films that allow selective cation or anion passage and are used in enrichment, desalinization, water electrolysis, and fuel cell applications. For example, perfluorosulfonate ionomer (Nafion®, produced by DuPont) membranes are highly chemically and thermally resistant and can therefore be used even in very toxic and dangerous processes such as those encountered in Cl_2 production, separation, electrodialysis, and fuel cell operation.

Table 1.1 Classification of fuel cells.[6]

Cell type	Typical electrolyte	Charge carrier	Major contaminants	Operation temperature (°C)	Electrical efficiency (%)	Techno-logical maturity[a]	Research activity[b]
Low temperature proton exchange membrane	Solid Nafion®	H^+	CO, H_2S	60–80	40–60	4	H
High temperature proton exchange membrane	Solid composite Nafion® Polybenzimidazole doped with H_3PO_4	H^+	CO	110–180	50–60	3	M
Alkaline	Aqueous KOH Anion-exchange membranes (AEMs)	OH^-	CO_2	Below zero–230	60–70	5	L
Direct methanol	Solid Nafion®	H^+	CO	Ambient–110	35–60	3	H
Phosphoric acid	Concentrated liquid H_3PO_4 in SiC	H^+	CO, siloxane, H_2S	160–220	36–45	5	M
Molten carbonate	Liquid alkali carbonates in $LiAlO_2$	CO_3^{2-}	Sulfides and halides	600–700	55–65	4	H
Solid oxide	Solid yttria-stabilized zirconia	O^{2-}	Sulfides	800–1000	55–65	3	H

[a]1: lowest, and 5: highest technological maturity relative to other fuel cell types.

[b]H: high; M: moderate; L: low.

Table 1.1 (continued)

Fuel cell type	Specific advantages	Specific disadvantages
Low temperature proton-exchange membrane	•Highly modular for most applications •High power density •Compact structure •Rapid start-up due to low temperature operation •Excellent dynamic response	•Complex water and thermal management •Low-grade heat •High sensitivity to contaminants •Expensive catalyst
High temperature proton-exchange membrane	•Simple water management •Simple thermal management •Fast reaction kinetics •High-grade heat •High tolerance to contaminants	•Accelerated stack degradation •Humidification issues •Expensive catalyst
Alkaline	•High electric efficiency due to fast reduction reaction kinetics •Wide range of operation temperature and pressure •Inexpensive and flexible catalyst •Relatively low cost	•Extremely high sensitivity to contaminants •Pure H_2 and O_2 required for operation •Low power density •Highly corrosive electrolyte leads to sealing issues •Complex and expensive electrolyte management for mobile electrolyte systems
Direct methanol	•Compact size •Simple system •High fuel volumetric energy density •Easy fuel storage and delivery •Simple thermal management for liquid methanol systems	•Low cell voltage and efficiency due to poor anode kinetics •Low power density •Lack of efficient catalysts for direct oxidation of methanol •Fuel and water crossover •Complex water management •High catalyst loading •High cost •Need for CO_2 removal system •Fuel toxicity
Phosphoric acid	•Technologically mature and reliable •Simple water management •Good tolerance to contaminants •High-grade heat	•Relatively slow start-up •Low power density •High sensitivity to contaminants •Expensive auxiliary systems •Low electrical efficiency •Relatively large system size •Electrolyte acid loss •Expensive catalyst •High cost
Molten carbonate	•High electrical efficiency •High-grade heat •High tolerance to contaminants •Possibility of internal reforming •Less strict material requirements •Fuel flexibility •Inexpensive catalyst	•Slow start-up •Low power density •Electrolyte corrosion and evaporative losses •Corrosion of metallic parts •Air crossover •Catalyst dissolution in electrolyte •Need for cathode CO_2 injection system
Solid oxide	•High electrical efficiency •High-grade heat •High tolerance to contaminants •Possibility of internal reforming •Eliminated electrolyte issues •Fuel flexibility •Inexpensive catalyst	•Slow start-up •Low power density •Strict material requirements •High thermal stresses •Sealing issues •Durability issues •High manufacturing costs

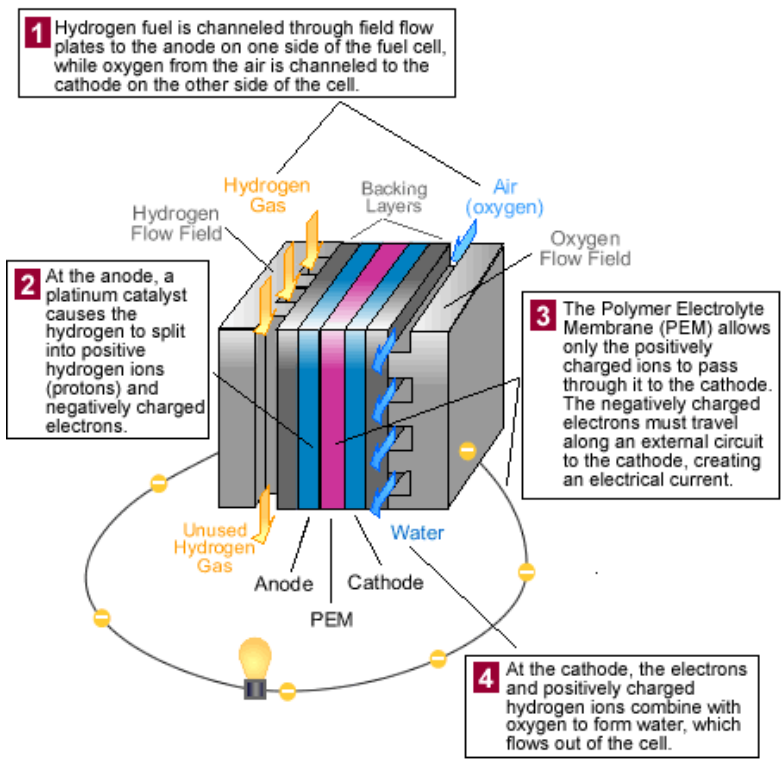

Figure 1.3 The operating principle of proton exchange membrane fuel cell.

Source: The official U.S. government source for fuel economy information (http://www.storedsolar.com/electrolysers.html).[7]

The operation of ion-exchange membranes is based on attractive or repulsive forces caused polar charges in pairs. For example, Nafion is a cation exchange membrane grafted with anionic sulfonate groups that selectively let through cations and do not let through anions because of anion-sulfonate repulsion. Conversely, anion-exchange membranes feature cationic functional groups that let through anions.[9] In order to be practically applicable, ion-exchange membranes need to exhibit high ionic conductivity, low gas permeability, and good mechanical and chemical stability.

Considering catalyst layers, the formation of a wide range of three-phase catalyst particle/ionomer/gas channel interfaces is required to maximize catalyst utilization (Figure 1.4).[10] For ion transfer in the MEA, polymer electrolytes are used as both membranes and catalyst binders, although the desired properties of these two components are quite different. Specifically, the electrolyte membrane should have excellent gas barrier properties to prevent hydrogen and air cross-over[11], while the electrolyte binder should be highly gas-permeable to enhance the electrocatalyst activity in the MEA electrode for reactions at the three-phase interfaces.[12]

.

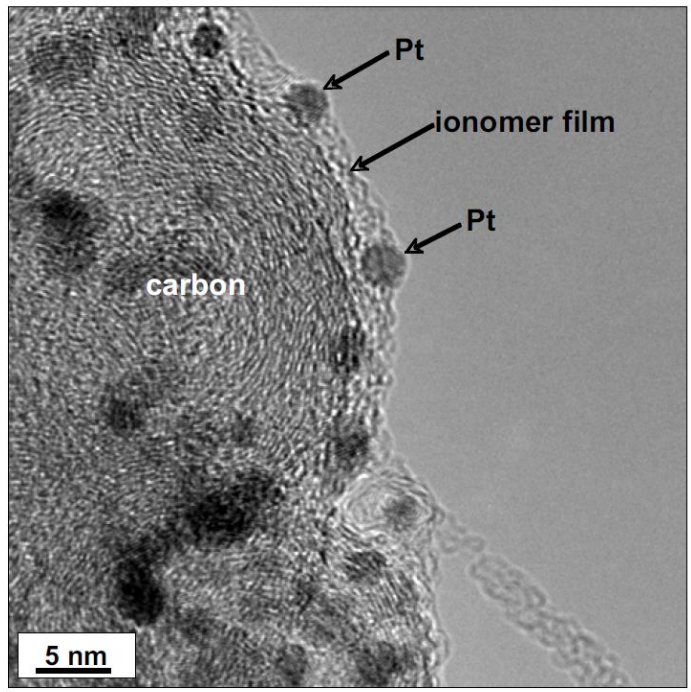

Figure 1.4 TEM image showing a model Pt/ionomer/C microstructure with the critical three-phase interfaces required to maximize Pt utilization.[10] (Adapted from K. More, et al., *ECS Trans.* (2006), **3**, 717-733.)

1.3. Anion exchange membrane fuel cells

Among fuel cells, PEMFCs exhibit the advantages of fast start-up time and low operating temperature, and hence feature the largest range of applications.[6] However, proton exchange membrane fuel cells exhibit the disadvantages of high fuel cross-over probability and high cost, as they contain expensive electrolyte membranes and noble metal catalysts.

Conversely, alkaline anion exchange membrane fuel cells (AEMFCs) feature the advantages of non-noble metal (Ni, Mn, Co, etc.) availability due to (i) the faster electrode reaction kinetics for the oxygen reduction reaction at high pH and (ii) the presence of an ion-conduction direction preventing fuel crossover.[13] In these cells, atmospheric O_2 is reduced on the cathode to produce hydroxide ions that are subsequently transferred through the electrolyte to the anode, where the oxidation of hydrogen to water takes place (Figure 1.5).[14] In conventional alkaline fuel cells with aqueous KOH as an electrolyte, performance degradation is mainly due to carbonation, i.e., to the blockage of pores and disruption of active layers caused by the precipitation of K_2CO_3 in electrodes. When aqueous KOH is replaced with an alkaline electrolyte membrane to afford AEMFCs, the inherent electrocatalytic advantages of alkaline fuel cells are retained, and typical problems associated with liquid electrolyte usage (such as K_2CO_3 precipitation or KOH solution leakage) are avoided. Additionally, thin and cheap metal bipolar plates can be used to address corrosion-derived problems at high pH.[15]

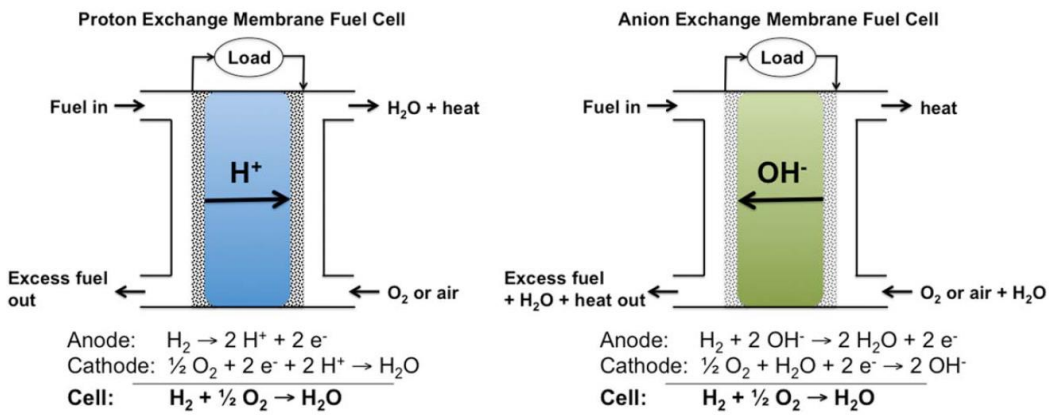

Figure 1.5 Schematic diagram of proton exchange membrane fuel cell and anion exchange fuel cell.[14] (Adapted from M.A. Hickner et al., *J. Polym. Sci., Part B: Polym. Phys.* (2013), **51**, 1727-1735.)

The commercialization of AEMFCs is hindered by the lack of materials satisfying the high performance and durability requirements to the same extent as the existing electrolytes and binders of proton-exchange membrane fuel cells. The transport of OH^-, as in the case of H^+, is believed to occur via a combination of the Grotthuss mechanism, hopping mechanism, vehicle diffusion mechanism, migration, and convection (Figure 1.6).[16, 17] However, at constant electrolyte thickness, the resistance of anion-exchange membranes exceeds that of proton-exchange membranes because of the smaller mobility of OH^- compared to that of H^+. For example, At a 100 V/m electric field and 298 K, the mobility of OH^- (20.64 μm/s) is only 57% of that of H^+ (36.23 μm/s).[18] Thus, AEMFC development is challenged by the poor alkaline stability and low cell performance of current AEMs and electrode ionomers.[16, 19, 20]

1.4. Subjects of this thesis

Most studies of alkaline membrane fuel cells have focused on electrolyte membranes and catalysts, leaving binders underexplored. As only a limited number of commercial (Tokuyama, Fumatech, Acta, etc.) ionomer solutions are available[21], this study aimed to develop a highly gas-permeable ionomer for alkaline AEMFCs.

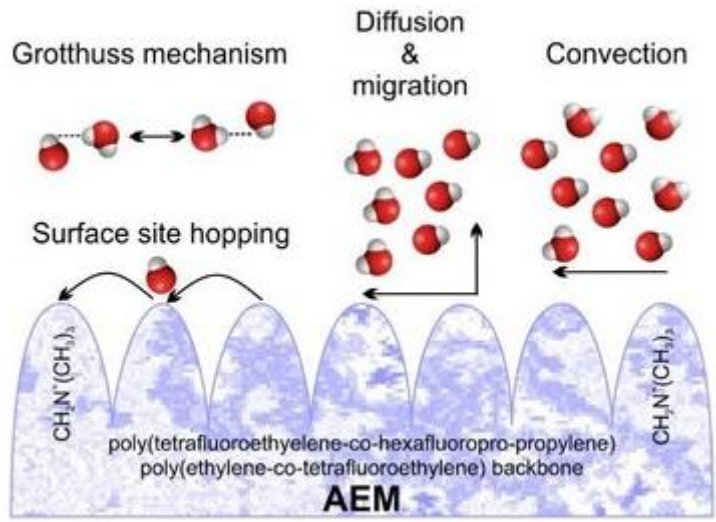

Figure 1.6 Possible OH^- transport mechanisms in AEMs: a combination of Grotthuss behavior, surface site hopping on quaternary side chains, diffusion and migration (concentration and/or potential gradients), and convection (pressure or electrostatic potential gradients).[16] (Adapted from L. Osmieri, et al., *Curr. Opin. Electrochem.* (2018), **9**, 240-256.)

Even though polymeric materials are used in both the membrane and catalyst binder to transfer ions, their roles in these components are different (Figure 1.7). The electrolyte membrane should exhibit good gas barrier properties to prevent hydrogen and air cross-over, while the binder has to be gas-permeable to enhance the electrochemical reactions at the electrode and facilitate the formation of three-phase (gas, catalyst, and electrolyte) boundaries.[22]

Figure 1.8 illustrates the pathway of oxygen diffusion in a PEMFC, showing that the "dead zones" are completely surrounded by carbon agglomerates/ionomer, i.e., catalysts in or around this zone are isolated from gases and cannot participate in the catalytic reaction.[23] However, despite the presence of dead zones, the active area of three-phase interfaces can be increased through the use of highly gas-permeable ionomers. There were no cases of gas permeability control of electrode binding ionomer for AEMFCs. This approach additionally allowed us to optimize AEMFC performance by efficiently establishing three-phase boundaries while avoiding problems caused by the adjustment of the length/amount of ionic side chains (Figure 1.9).[24]

Herein, considering the fact that the spirobiindane structure is thought to be suitable for the fabrication of electrode-binding ionomers with high gas permeability (Figure 1.10)[25, 26], we synthesized a poly(arylene ether sulfone) with a spirobiindane moiety in the polymer backbone. Compared to the common PES, the SBI-PES showed higher gas permeability due to the increased fractional free volume related to the internal void volume of the spirobiindane unit. Moreover, we fabricated an MEA using a series of hydroxide-conducting PESs bearing spirobiindane moieties and tetra(quaternary

ammonium) pendant groups and evaluated the single-cell performance of the corresponding alkaline membrane fuel cells, revealing that the hydroxide-conducting spirobiindane-based PES achieved better cell performance than the non-spirobiindane-based one.

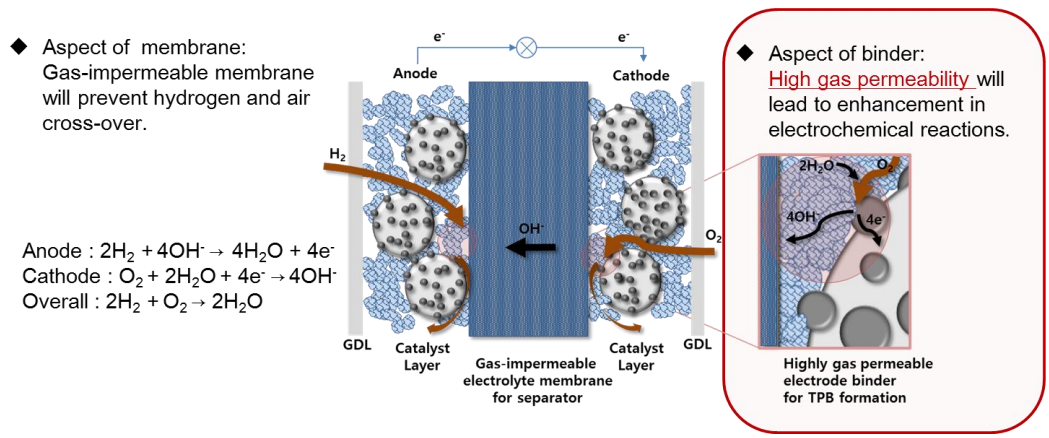

Figure 1.7 Gas-impermeable electrolyte membrane and highly gas-permeable electrode-binding ionomer for AEMFCs.

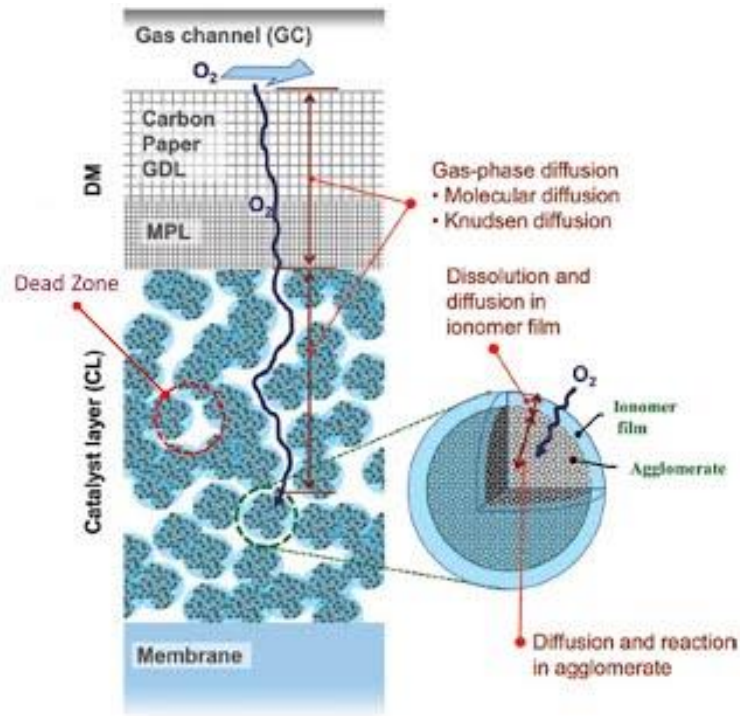

Figure 1.8 Schematic of oxygen diffusion pathway in a PEMFC.[23] (Adapted from N. Nonoyama et al., *J. Electrochem. Soc* (2011), **158**, B416-B423.)

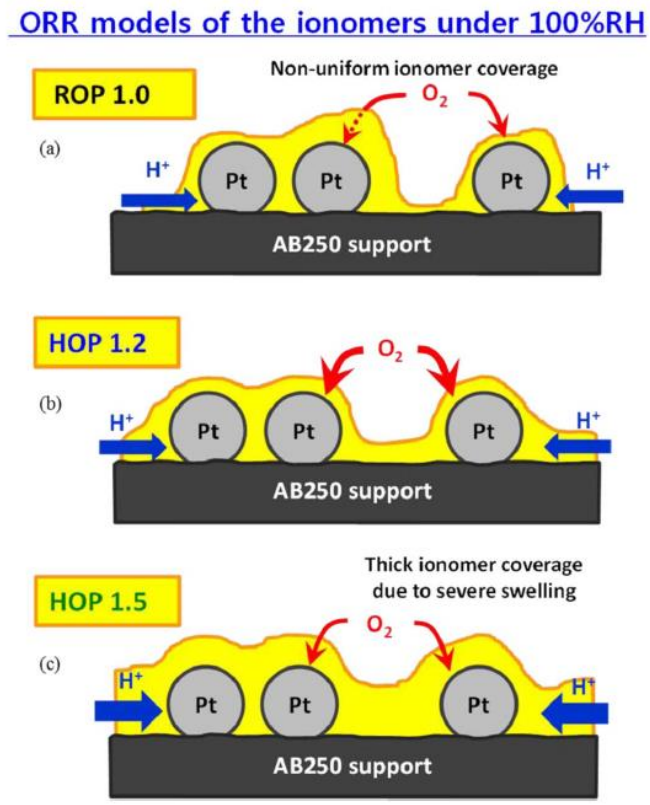

Figure 1.9 Ionomer coverage for different ionomer IEC values.[24] (Adapted from R. Shimizu et al., *J. Electrochem. Soc.* (2018), **165**, F3063-F3071.)

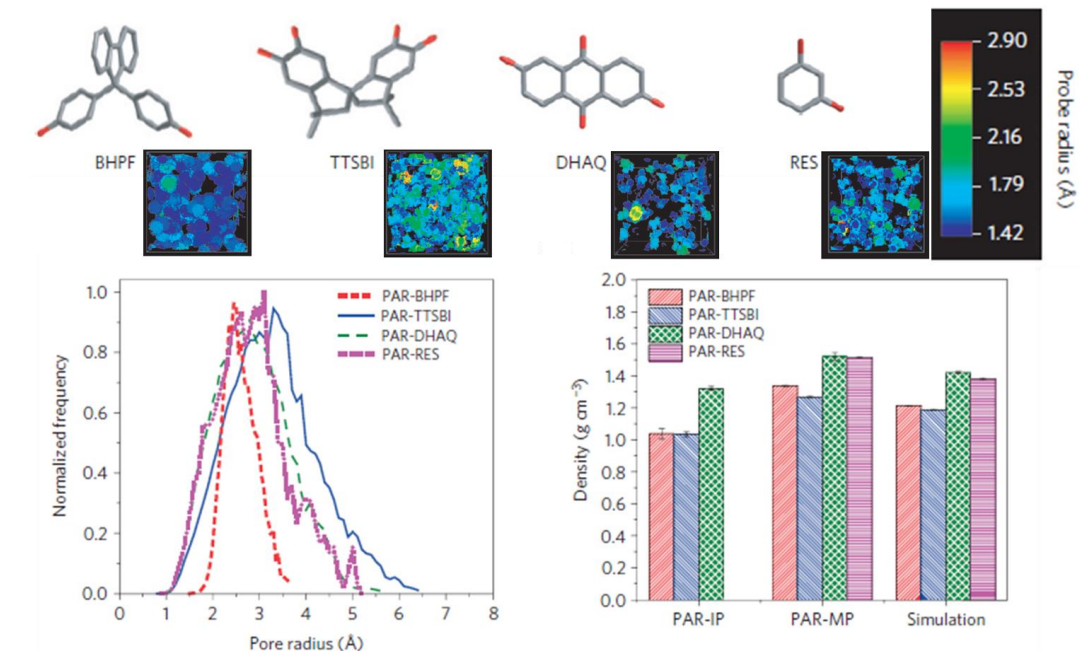

Figure 1.10 Structural analysis of amorphous polymer models.[25] (Adapted from M.F. Jimenez-Solomon, et al., *Nat. Mater.* (2016), **15**, 760-767.)

1.5. References

[1] N.L. Panwar, S.C. Kaushik, S. Kothari, Role of renewable energy sources in environmental protection: A review, *Renew. Sust. Energ. Rev.* (2011), **15**, 1513-1524.

[2] S. Kharel, B. Shabani, Hydrogen as a long-term large-scale energy storage solution to support renewables, *Energies* (2018), **11**, 2825-2841.

[3] N. Behling, M.C. Williams, S. Managi, Fuel cells and the hydrogen revolution: Analysis of a strategic plan in Japan, *Econ. Anal. Pol.* (2015), **48**, 204-221.

[4] Stored Solar, *electolysers*, http://www.storedsolar.com/electrolysers.html.

[5] Energy Technologies Area, *Hydrogen: The energy carrier of the future*, https://eta.lbl.gov/news/article/hydrogen-energy-carrier-future.

[6] O.Z. Sharaf, M.F. Orhan, An overview of fuel cell technology: fundamentals and applications, *Renew. Sust. Energ. Rev.* (2014), **32**, 810-853.

[7] The official U.S. government source for fuel economy information, *How fuel cells work*, https://www.fueleconomy.gov/feg/fcv_PEM.shtml.

[8] H.-J. Kim, Single cell for proton exchange membrane fuel cells (PEMFCs), in: D. Stolten, R. C. Samsun, N. Garland (Eds.), Fuel cells: Data, facts, and figures, Wiley-VCH: Weinheim (2016), pp. 135-140.

[9] Y. Tanaka, Mass transport in a boundary layer and in an ion exchange membrane: Mechanism of concentration polarization and water dissociation, *Russ. J. Electrochem.* (2012), **48**, 665-681.

[10] K. More, R. Borup, K. Reeves, Identifying contributing degradation phenomena in PEM fuel cell membrane electrode assemblies via electron microscopy, *ECS Trans.* (2006), **3**, 717-733.

[11] J. Catalano, T. Myezwa, M.G. De Angelis, M.G. Baschetti, G.C. Sarti, The effect of relative humidity on the gas permeability and swelling in PFSI membranes, *Int. J. Hydrogen Energy* (2012), **37**, 6308-6316.

[12] G. Sasikumar, J.W. Ihm, H. Ryu, Dependence of optimum Nafion content in catalyst layer on platinum loading, *J. Power Sources* (2004), **132**, 11-17.

[13] Q. He, E. J. Cairns, Review—Recent progress in electrocatalysts for oxygen reduction suitable for alkaline anion exchange membrane fuel cells, *J. Electrochem. Soc.* (2015), **162**, F1504-F1539.

[14] M.A. Hickner, A.M. Herring, E.B. Coughlin, Anion exchange membranes: Current status and moving forward, *J. Polym. Sci., Part B: Polym. Phys.* (2013), **51**, 1727-1735.

[15] D.R. Dekel, Review of cell performance in anion exchange membrane fuel cells, *J. Power Sources* (2018), **375**, 158-169.

[16] L. Osmieri, L. Pezzolato, S. Specchia, Recent trends on the application of PGM-free catalysts at the cathode of anion exchange membrane fuel cells, *Curr. Opin. Electrochem.* (2018), **9**, 240-256.

[17] S.C. Ramírez, R.R. Paz, Hydroxide Transport in anion-exchange membranes for alkaline fuel cells (2018).

[18] P. Atkins, "Physical Chemistry 7th Ed." (2002).

[19] S. Gottesfeld, D.R. Dekel, M. Page, C. Bae, Y. Yan, P. Zelenay, Y.S. Kim, Anion exchange membrane fuel cells: current status and remaining challenges, *J. Power Sources* (2018), **375**, 170-184.

[20] C.G. Arges, L. Zhang, Anion exchange membranes' evolution toward high hydroxide ion conductivity and alkaline resiliency, *ACS Appl. Energy Mater.* (2018), **1**, 2991-3012.

[21] X. Gao, H. Yu, J. Jia, J. Hao, F. Xie, J. Chi, B. Qin, L. Fu, W. Song, Z. Shao, High performance anion exchange ionomer for anion exchange membrane fuel cells, *RSC Advances* (2017), **7**, 19153-19161.

[22] Y.J. Yoon, T.-H. Kim, D.M. Yu, J.-Y. Park, Y.T. Hong, Modification of hydrocarbon structure for polymer electrolyte membrane fuel cell binder application, *Int. J. Hydrogen Energy* (2012), **37**, 13452-13461.

[23] N. Nonoyama, S. Okazaki, A Z. Weber, Y Ikogia, T. Yoshida, Analysis of Oxygen-Transport Diffusion Resistance in Proton-Exchange-Membrane Fuel Cells, *J. Electrochem. Soc* (2011), **158**, B416-B423.

[24] R. Shimizu, Y.-C. Park, K. Kakinuma, A. Iiyama, M. Uchida, Effects of both oxygen permeability and ion exchange capacity for cathode ionomers on the performance and durability of polymer electrolyte fuel cells, *J. Electrochem. Soc.* (2018), **165**, F3063-F3071.

[25] M.F. Jimenez-Solomon, Q. Song, K.E. Jelfs, M. Munoz-Ibanez, A.G. Livingston, Polymer nanofilms with enhanced microporosity by interfacial polymerization, *Nat. Mater*. (2016), **15**, 760-767.

[26] J.E. Chae, B.H. Kim, J.H. Noh, J. Jung, J.-Y. Kim, J.H. Jang, S.J. Yoo, H.-J. Kim, S.Y. Lee, Effect of the spirobiindane group in sulfonated poly(arylene ether sulfone) copolymer as electrode binder for polymer electrolyte membrane fuel cells, *J. Ind. Eng. Chem.* (2017), **47**, 315-322.

Chapter 2. Spirobiindane-based microporous poly(arylene ether sulfone)s as polymeric binder on alkaline anion exchange membrane fuel cells

2.1. Background

The membrane electrode assembly (MEA) in polymer electrolyte membrane fuel cells (PEMFC) is the most important component that determines the whole cell performance.[1] Polymer electrolytes are used as both a membrane and catalyst binder for ion transfer in the MEA. However, the required properties of the membrane and the catalyst binder are quite different. The electrolyte membrane should have high gas barrier property to prevent hydrogen and air cross-over,[2] while the electrolyte binder should be gas-permeable to enhance the electro-catalyst activity in the electrode of the MEA.[3] A highly gas-permeable binder can enhance a reaction at the three-phase boundary among reactant gases, the catalyst, and electrolytes in the electrode.

Poly(arylene ether sulfone)s (PESs) are one of the promising hydrocarbon-based polymer electrolytes for PEMFCs owing to their good chemical resistance, mechanical properties, and thermal stabilities[4-6] and especially low gas permeabilities. Therefore, PES-based electrolytes are excellent materials for a

membrane. However, they show very low cell performance as binders.[7]

Polymer materials have also been investigated for their gas separation applications. The polymer structure influences its permeability and selectivity for different gas pairs.[8] To obtain high gas permeability, many researchers have studied the influence of distorted groups on the polymer backbone and bulky pendant groups to increase the fractional free volume (FFV) between polymer chains.[9-11] Representative cases of the approach to improve the gas permeation behavior were about the application of spirobiindane,[12] hexafluoro,[13] and cardo moieties.[14]

Very few studies have focused on improving cell performance by increasing the gas permeability of the binder.[15-17] Previously, we also synthesized sulfonated PES binders containing spirobiindane groups for proton-exchange membrane fuel cell electrodes. The highly gas-permeable polymer electrolyte binder with spirobiindane moiety showed higher cell performance than those without the moiety.[15]

Alkaline anion exchange membrane fuel cells (AEMFC) have been studied intensively for the last 10 years because of their advantage of being low-cost catalysts.[18-20] However, most studies focused on electrolyte membranes[21] and catalysts and there are only a few studies on binders.[22-25] The purpose of this study is to develop a new catalyst binding polymer and an electrode binder in the MEA for AEMFC. We synthesized a new spirobiindane modified poly(arylene ether sulfone) (SBI-PES) and a series of PESs (QOH-SBIs), which have spirobiindane and tetra(quaternary ammonium) hydroxide pendant moieties as

electrode binders.

The gas permeability of SBI-PES was compared to that of the pristine polymer to investigate the effect of spirobiindane units. A role of spirobiindane group to the binder structure is investigated. Wide angle X-ray diffraction (WAXD) was used to find out the inter-chain spacing formed by a difference in chain thickness of two alternating repeating units, thick spirobiindane unit and thin arylene ether sulfone unit. An effect of spirobiindane unit to the chain conformation was also investigated in a solution by the small angle neutron scattering (SANS) measurement.

We fabricated the MEA for AEMFC using a series of QOH-SBIs as an electrode binder. QOH-SBIs show better cell performance than the polymers without spirobiindane unit. As a result, high gas permeability is an essential factor that electrode binders must have, and future research on this issue should be continued.

2.2. Experimental

2.2.1. Materials

Bisphenol A, 4,4'-difluorodiphenylsulfone, 4,4'-dihydroxydiphenyl ether, dimethylamine solution (33 wt%), formaldehyde solution (37 wt%), cesium carbonate, methanesulfonic acid, iodomethane, anhydrous *N*-methyl-2-pyrrolidone, anhydrous toluene, anhydrous *N,N*-dimethylacetamide were purchased from Sigma-Aldrich and used without additional purification. 4,4'-Biphenol was purchased from TCI and used after recrystallization. Ethanol and isopropanol were purchased from Daejung and Honeywell, respectively. Prior to synthesis, all monomers and polymers were dried overnight in a vacuum oven at 60 °C. For the single cell test, the electrocatalyst was purchased from Tanaka Kikinzoku Kogyo (K. K.). Used anion exchange membranes (A201) were from Tokuyama Corporation and gas diffusion layers (Sigracet® 39BC) were from SGL Carbon.

2.2.2. Characterization and methods

^{1}H NMR spectra were obtained using Bruker 400 MHz AVANCE-III spectrometer with synthesized products dissolved in deuterated dimethylsulfoxide or chloroform. Two drops of trifluoroacetic acid-*d* were added to the NMR samples so that water peak can't overlap with signals of samples.

$$\mathrm{DF} = \frac{\text{Peak area ratio of N-CH}_3}{\text{Peak area ratio of aromatic H}} \quad (1)$$

$$IEC_{NMR} = \frac{DF \times 4 \text{ equiv.}}{DF \times MW_{R.U. \text{ of } QOH} + ((100-DF) \times MW_{R.U. \text{ of SBI or BP}})} \quad (2)$$

The molecular weight and polydispersity index of the polymers were analyzed by gel permeation chromatography (Waters 2414 refractive index detector) using 0.05 M Li Br in NMP as an eluent. The analysis was conducted at 40 °C and 1.0 mL min^{-1} flow rate. Thermal gravimetric analysis was performed using Q50 apparatus (TA Instruments). Under N_2 atmosphere, 5 mg polymer was heated at a heating rate of 10 °C min^{-1} to 900 °C. The FT-IR spectra were recorded in ATR mode by Lambda Scientific FTIR 7600. The mechanical properties of polymer membranes were measured using QC-508E (Cometech). The rectangular samples with the test area of 2 cm (l_0) × 1 cm (w_0) × 30 μm (d_0) were stretched at a rate of 0.5 mm min^{-1} at room temperature. The tensile strength (σ) and elongation percentage (ε) were obtained from the equations. Young's modulus was determined from the initial slope of the stress–strain curve. All the values are the average values of two specimen measurement results. The experiment was carried out three times and the results were averaged.

$$\sigma = \frac{F}{w_0 \times d_0} \quad (3)$$

$$\varepsilon = \frac{l - l_0}{l_0} \times 100 \quad (4)$$

Gas permeation test was conducted with membrane samples (effective area (A): 3.14 cm^2 and thickness (d): 30 μm or 100 μm) and 760 mmHg pressure (P_{feed}) of each gas (He, H_2, CO_2, O_2, N_2, CH_4) at 35 °C (T)(Figure 2.1).[26]

$$P = \frac{V M_{gas} d}{P_{feed} R T A \rho} \times \frac{dp}{dt} \quad (5)$$

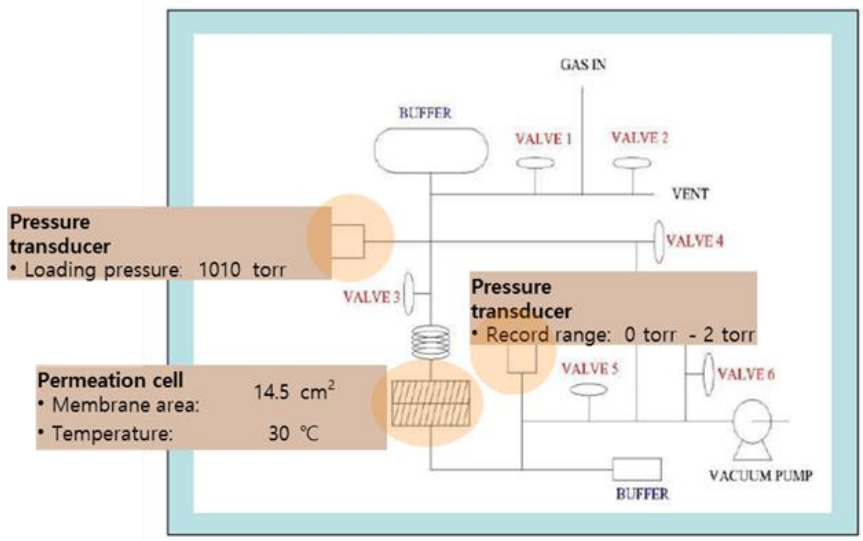

Figure 2.1 Schematic diagram of proton exchange membrane fuel cell and anion exchange fuel cell.

$$D = \frac{d^2}{6\theta} \quad (6)$$

$$P = D \times S \quad (7)$$

$$\alpha_{A/B} = \frac{P_A}{P_B} \quad (8)$$

where V (cm^3) is volume of measurement device at bottom of the membrane, M_{gas} (g mol^{-1}) is molecular weight of permeating gas, ρ (g cm^{-3}) is density of permeating gas, R (L mmHg K^{-1} mol^{-1}) is the gas constant, and dp/dt is the slope plotted from change of permeated gas pressure over time. θ was x-intercept obtained from the constant slope section of the time-lag graph by extrapolation.

The water uptake was determined by measuring the weight change of the membranes immersed in deionized water at 30 °C and 80 °C for 24 h. Prior to the test, all the polymers were dried overnight in a vacuum oven at 60 °C. This experiment was repeated three times and the results were averaged.

$$\text{Water uptake} = \frac{W_{wet} - W_{dry}}{W_{dry}} \times 100 \quad (9)$$

$IEC_{titration}$ values were determined by Mohr titration.[27] 0.05 g of OH^- form sample was immersed in 15 mL of 0.5 M HCl solution for 8 h and washed with DI water. Then the Cl^- form sample was immersed in 15 mL of 0.2 M $NaNO_3$ for 8 h. The $NaNO_3$ solution was collected as titrand and titrated with 0.1 M $AgNO_3$. 5% K_2CrO_4 solution was used as indicator for this titration. The IEC was calculated from the weight of the sample and the moles of Ag^+ consumed in the titration. The

experiment was conducted twice and the results were averaged.

$$\mathrm{IEC}_{\mathrm{titration}} = \frac{V_{\mathrm{AgNO_3}} \times M_{\mathrm{AgNO_3}}}{W_{\mathrm{dry}}} \quad (10)$$

To obtain the conductivity values, membrane samples (4 cm × 1 cm × 30 μm) were prepared. The samples were inserted in a four-probe conductivity cell and the cell was placed in a chamber. Impedance analysis was carried out while controlling humidity and temperature. Applying a sinusoidal current signal (amplitude: 1 μA), the signal frequency was scanned from 5 MHz to 1 Hz (SP-300, Bio-Logic Science Instruments). The conductivity was calculated using the ohmic resistance (R), the cross-sectional area (A) of the membrane sample, and the distance (L) between the two voltage sensing probes. The ohmic resistance was determined from the x-axis intercept at the higher frequency region in the Nyquist plot.

$$\mathrm{Conductivity} = \frac{L}{RA} \quad (11)$$

The X-diffraction was measured at room temperature using an X-ray diffractometer (model: PANalytical Empyrean) with the following operating conditions: Cu Kα, 45 kV and 40 mA, step size 0.013° in the range of 2θ = 5–80°.

The liquid samples with a concentration of 0.0025 g mL^{-1} were loaded into a quartz cell with a path length of 1 mm. Small angle neutron scattering (SANS) measurements were performed on the NGB-30m instruments, respectively, at the National Institute of Standards Technology Center for Neutron Research (NCNR). SANS was measured at three sample-to-detector distances (1 m, 4 m, and 13 m) to cover a scattering vector (Q) range of 0.003–0.410 $Å^{-1}$ with a neutron wavelength

of λ = 6 Å. The isotropic 2D scattering pattern was corrected to an absolute scale (unit cm^{-1}) by modifying the empty quartz cell scattering, environmental background, transmission, and beam flux. The 2D scattering pattern was converted to the azimuthally-averaged 1D scattering profile (*i.e.*, macroscopic cross-section versus scattering vector). The data reduction was performed using the NCNR Data Reduction Macro and Analysis package.[28]

2.2.3. Synthetic procedures

Synthesis of spirobiindane bisphenol

Scheme 2.1 shows the synthetic procedure of spirobiindane bisphenol and polymer series. Bisphenol A (40.00 g, 0.175 mol) was added to methanesulfonic acid (70 mL). The solution was stirred at 25 °C for 96 h and precipitated by pouring it to iced deionized water at 10 °C. The product was obtained by recrystallization in ethanol (yield: 83%). ^{1}H NMR (400 MHz, DMSO-d_6, δ): 2.29–2.65 (m, 12H, C-H_3 of spirobiindane), 3.19–3.51 (m, 4H, C-H of spirobiindane), 7.19–8.22 (m, 6H, Ar H).

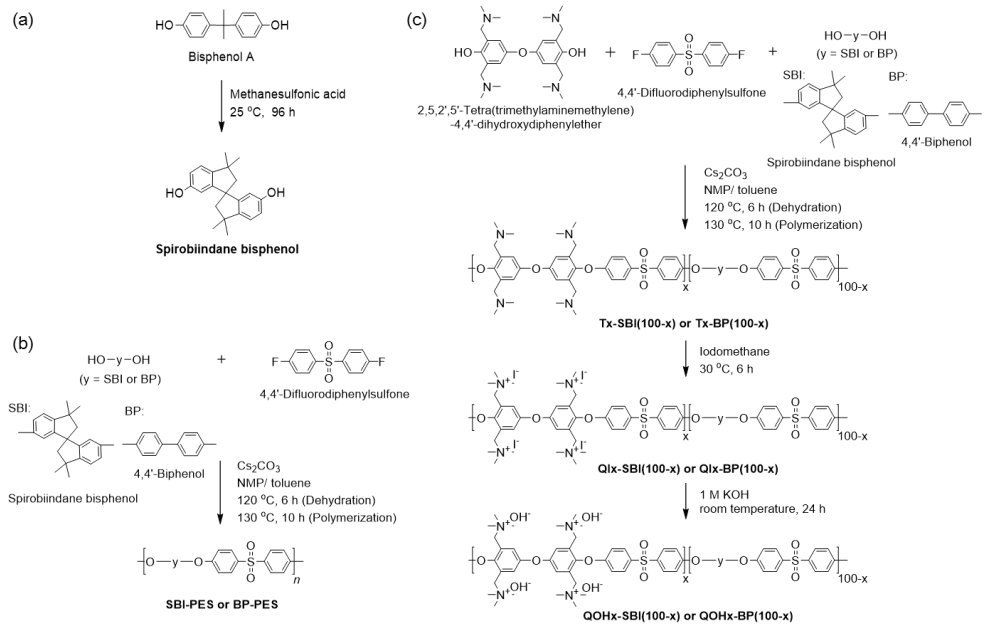

Scheme 2.1 Synthetic procedure of a) spirobiindane bisphenol, b) spirobiindane-PES / biphenyl-PES, and c) QOHx-SBI(100-x)s / QOHx-BP(100-x)s.

Synthesis of PES containing spirobiindane group

Spirobiindane bisphenol (1.87 g, 6 mmol), 4,4'-difluorodiphenyl sulfone (1.54 g, 6 mmol), anhydrous Cs_2CO_3 (4.11 g, 12.6 mmol), anhydrous NMP (22 mL), and toluene (6 mL) were mixed in a 250-mL four-necked round-bottomed flask equipped with a Dean-Stark trap, mechanical stirrer, argon gas inlet, and thermometer. For dehydration, the reaction mixture was heated to 120 °C for 6 h. After toluene and water had been distilled off, the temperature was raised to 130 °C and the mixture was stirred for 10 h. The solution was poured into ethanol to precipitate the product. The polymer was washed with ethanol and deionized water (yield: 96%). ^{1}H NMR (400 MHz, DMSO-d_6, δ): 1.23–1.49 (m, 12H, C-H$_3$ of spirobiindane), 2.19–2.52 (m, 4H, C-H of spirobiindane), 6.35–8.01 (m, 14H, Ar H).

Synthesis of PES containing biphenyl group

4,4'-Biphenol (8.46 g, 45.0 mmol), 4,4'-difluorodiphenyl sulfone (11.56 g, 45.0 mmol), anhydrous Cs_2CO_3 (30.82 g, 94.5 mmol), anhydrous NMP (140 mL), and toluene (45 mL) were mixed in a 500-mL four-necked round-bottomed flask equipped with a Dean-Stark trap, mechanical stirrer, argon gas inlet, and thermometer. For dehydration, the reaction mixture was heated to 120 °C for 6 h. After toluene and water had been distilled off, the temperature was raised to 130 °C and the mixture was stirred for 10 h. The solution was poured into ethanol to precipitate the product. The polymer was washed with ethanol and deionized water (yield: 99%). ^{1}H NMR (400 MHz, DMSO-d_6, δ): 7.05–8.01 (m, 16H, Ar H).

Synthesis of 2,5,2',5'-tetra(trimethylaminemethylene)-4,4'-dihydroxydiphenylether (TADHDPE)

4,4'-Dihydroxydiphenyl ether was dissolved in ethanol. Dimethylamine solution (33wt% in ethanol) and formaldehyde solution (37wt% in H_2O) were added. The reaction mixture was stirred at 70 ^oC for 24 h. Recrystallizations from ethanol gave the product as buff powder like preveously synthesized.[5]

Synthesis of poly(arylene ether sulfone) containing quaternary ammonium iodide and spirobiindane groups (QI30-SBI70)

TADHDPE (3.91 g, 9 mmol), spirobiindane bisphenol (6.54 g, 21 mmol), 4,4'-difluorodiphenyl sulfone (7.7 g, 30 mmol), Cs_2CO_3 (20.55 g, 63 mmol), anhydrous NMP (118 mL), and toluene (30 mL) were mixed in a 250-mL four-necked round-bottomed flask equipped with a Dean-Stark trap, mechanical stirrer, argon gas inlet, and thermometer. For dehydration, the reaction mixture was heated to 120 °C for 6 h. After toluene and water had been distilled off, the temperature was raised to 130 °C and the mixture was stirred for 10 h. The solution was poured into ethanol to precipitate the product. The polymer was washed with ethanol and deionized water and then dried at 60 °C for overnight in a vacuum oven (yield: 94 %).

For tertiary amine-to-quaternary ammonium conversion, iodomethane (2.51 mL, 2 equiv. of the tertiary amine groups) was added to the solution of PES containing tertiary amine groups (10.00 g) in DMAc (150 mL) in a 250-mL one-necked round-bottomed flask. The reactants were stirred at 30 °C for 6 h and then poured into ethanol. The product was washed with ethanol several times (yield: 81%). ^1H

NMR (DMSO-d_6, δ): 1.13–1.52 (m, 84H, C-H_3 of spirobiindane), 2.07–2.47 (m, 28H, C-H of spirobiindane), 3.02–3.43 (br, 72H, –N^+–CH_3), 3.73–4.91 (br, 24H, –CH_2–N^+–), 6.26–8.36 (m, 113H, Ar H).

Synthesis of poly(arylene ether sulfone) containing quaternary ammonium iodide and biphenyl groups (QI30-BP70)

TADHDPE (3.91 g, 9 mmol), 4,4'-biphenol (3.95 g, 21 mmol), 4,4'-difluorodiphenyl sulfone (7.70 g, 30 mmol), Cs_2CO_3 (20.55 g, 63 mmol), anhydrous NMP (108 mL), and toluene (30 mL) were added to a 250-mL four-necked round-bottomed flask equipped with a Dean-Stark trap, mechanical stirrer, argon gas inlet, and thermometer. For dehydration, the reaction mixture was heated to 120 °C for 6 h. After toluene and water had been distilled off, the temperature was raised to 130 °C and the mixture was stirred for 10 h. The solution was poured into ethanol to precipitate the product. The polymer was washed with ethanol and deionized water and then dried at 60 °C for overnight in vacuum oven (yield: 98%).

For tertiary amine-to-quaternary ammonium conversion, iodomethane (3.25 mL, 2 equiv. of the tertiary amine groups) was added to the solution of PES containing tertiary amine groups (10.00 g) in DMAc (150 mL) in a 250-mL one-necked round-bottomed flask. The reactants were stirred at 30 °C for 6 h and then poured into ethanol. The product was washed with ethanol several times (yield: 84%). ^{1}H NMR (DMSO-d_6, δ): 2.82–3.55 (br, 108H, –N^+–CH_3), 3.80–4.73 (br, 24H, –CH_2–N^+–), 6.59–8.26 (m, 148H, Ar H).

2.2.4. Membrane fabrication

The polymers were dissolved in NMP (5 wt%). The polymer solutions were then filtered using 0.45-μm PTFE cartridges. The solutions (17.65 g or 5.29 g) were loaded into glass Petri dishes (diameter: 9.05 cm) and the solvents were evaporated at 80 °C for 48 h and 100 °C for 4 h in a vacuum oven. The membranes were peeled off by swelling with deionized water. The thickness of the membranes was controlled at 100 μm or 30 μm. To remove the remaining solvent in the membranes, the membranes were soaked in methanol for 48 h and then in hexane for 24 h.

2.2.5. Counter ion exchange from iodide form to hydroxide form

To convert the I^- form membranes into OH^- form membranes, the membranes were soaked in 1 M KOH solution at room temperature. After 24 h, the membranes were washed to bring them to neutral pH and preserved in deionized water.

2.2.6. Binder solution preparation

The polymers were dissolved in DMAc (5 wt%) and the polymer solutions were filtered using 0.45-μm PTFE cartridges.

2.2.7. Fabrication of the membrane electrode assembly (MEA) for single-cell test

The catalyst slurry for the electrodes was prepared by dispersing 46.5 wt% Pt/C electrocatalyst (13 mg) in the synthetic PES Ionomer solution (111 mg) and

isopropanol (3 mL). This catalyst slurry was coated on both sides of the anion exchange membrane (A201), 5 cm^2 in size, by a spraying method. The Pt loading amount was 0.4 mg cm^{-2} on each side of the electrode and the ionomer content was 30 wt%. The catalyst coated membrane, gas diffusion layers, bipolar plates, and end plates were assembled by a torque wrench for 70 kgf cm^{-2}.

2.2.8. Fuel cell tests of membrane electrode assemblies (MEAs)

A 5-cm^2 single-cell consisting of an MEA was operated at 60 °C and 100% RH. H_2 and O_2 gases were fed to the anode and cathode with flow rates of 200 mL min^{-1} and 400 mL min^{-1}, respectively. After the steady-state was reached, the cell was activated at 0.4 V and the *I–V* polarization curves were plotted.

2.3. Results and discussion

2.3.1. Synthesis and characterization of spirobiindane modified poly(arylene ether sulfone) (SBI-PES)

The spirobiindane-PES homopolymer (SBI-PES) (Figure 2.2a) was synthesized from spirobiindane bisphenol (SBIBP) and 4,4'-difluorodiphenyl sulfone (DFDPS) in *N*-methyl-2-pyrrolidone (NMP) with cesium carbonate by an aromatic nucleophilic condensation reaction at 130 °C for 10 h.[29] The monomer containing the spirobiindane group was synthesized according to a previously reported mechanism.[30] For comparison, biphenyl-PES (BP-PES) (Figure 2.2b) was prepared under the same reaction conditions from 4,4'-biphenol and DFDPS. The polymer structures were confirmed and identified by ^{1}H NMR as shown in Figure 2.3.

Both SBI-PES and BP-PES polymers have high molecular weights and good mechanical properties (Table 2.1). Even though the tensile strength and elongation of SBI-PES are lower than those of BP-PES, the SBI-PES has good mechanical strength and is easy to manufacture as a free-standing membrane.

Gas permeability (*P*), diffusivity coefficients (*D*), solubility (*S*), and selectivity of membranes were determined by a time-lag method (Table 2.2 and Table 2.3).[31] Compared to BP-PES, SBI-PES showed high gas permeability owing to the increased fractional free volume that is the inter-chain spacing between spirobiindane and arylene ether sulfone groups. The bulky spirobiindane unit in the

main-chain improved the gas permeation properties. The gas permeability trend corresponds to the order of kinetic diameter of gas molecules. Poly(arylene ether sulfone) containing spirobiindane groups represent one order or half an order of higher gas permeability value than previously reported poly(arylene ether sulfone) containing phthalimide side group series.[14]

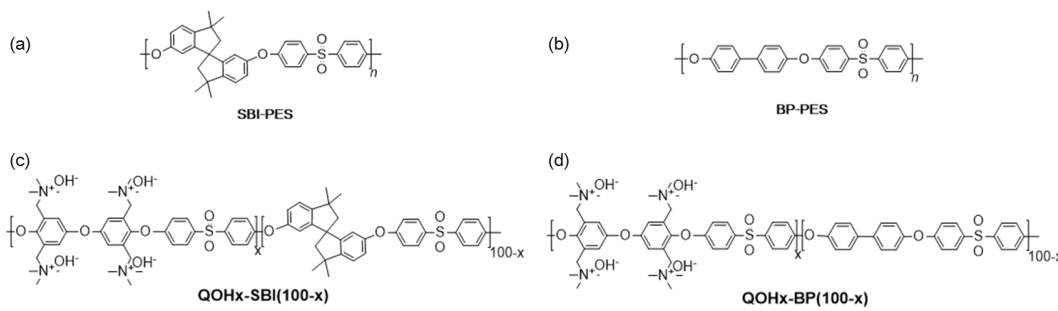

Figure 2.2 Chemical structure of a) SBI-PES, b) BP-PES, c) QOHx-SBI(100-x)s and d) QOHx-BP(100-x)s.

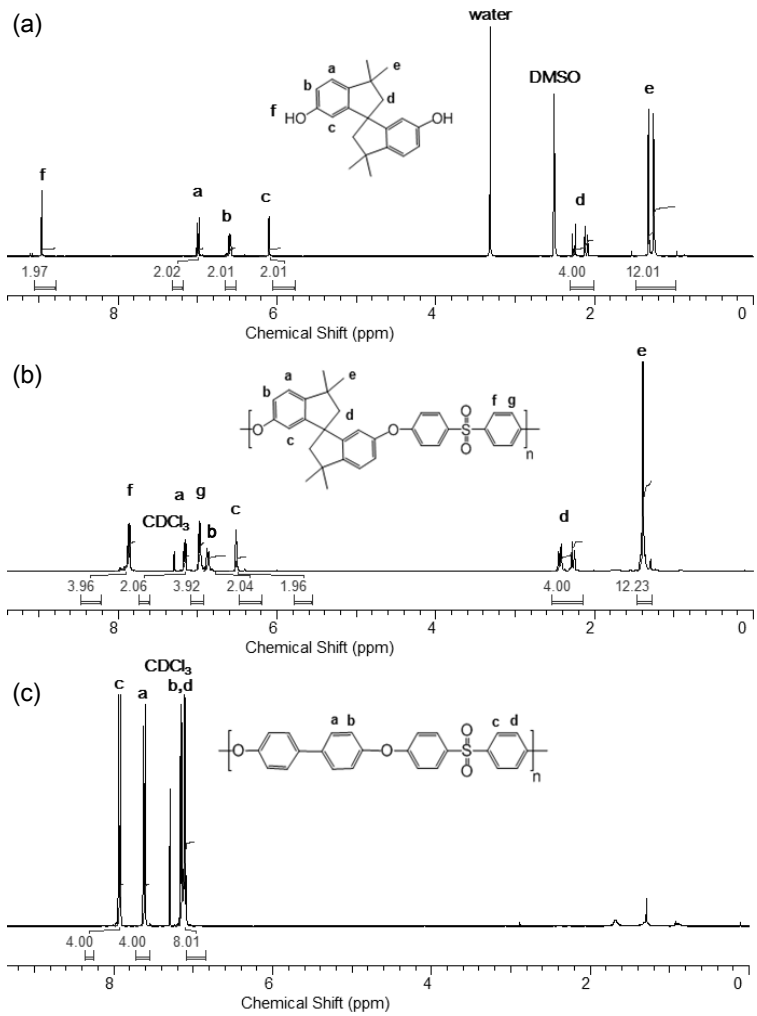

Figure 2.3 [1]H NMR spectra of a) spirobiindane bisphenol, b) SBI-PES, and c) BP-PES.

Table 2.1 Physical properties of SBI-PES and BP-PES.

Sample	M_n (g mol^{-1})	PDI	Tensile strength at break (MPa)	Young's modulus (GPa)	Elongation at break (%)
SBI-PES	71,150	1.26	17.2 ± 5.0	1.9 ± 0.3	9.5 ± 4.0
BP-PES	82,414	1.31	50.7 ± 2.9	0.6 ± 0.2	92.3 ± 34.7

Table 2.2 Gas permeability (*P*) and diffusivity coefficients (*D*) of the membranes.

Sample	Permeability (Barrer[a)])						Diffusion coefficient (10^{-9} cm^2 s^{-1})				
	He	H_2	CO_2	O_2	N_2	CH_4	He	H_2	CO_2	O_2	N_2
SBI-PES	146.81	184.14	89.69	30.06	10.84	13.40	4771.21	5256.38	60.59	215.58	80.84
BP-PES	4.44	3.77	1.38	0.26	0.05	0.05	196.67	394.68	3.31	9.15	2.00

[a)] Barrer = 10^{-10} cm^3 (STP) cm cm^{-2} s^{-1} $cmHg^{-1}$

Table 2.3 Gas solubility (*S*) and selectivity of the membranes.

Sample	Solubility (10^{-2} cm^3 (STP) cm cm^{-3} $cmHg^{-1}$)						Selectivity					
	He	H_2	CO_2	O_2	N_2	CH_4	H_2/CO_2	H_2/O_2	CO_2/O_2	H_2/N_2	CO_2/N_2	O_2/N_2
SBI-PES	0.23	0.27	11.25	1.06	1.02	3.52	2.05	6.13	0.28	16.99	8.27	2.77
BP-PES	0.17	0.07	3.16	0.21	0.18	0.77	2.74	14.50-	5.34	79.63	29.11	5.45

The internal micropores were determined from the WAXD measurement. The WAXD spectra of SBI-PES and BP-PES are shown in Figure 2.4. No crystalline peaks were observed and only broad amorphous halos are shown. This confirms that both SBI-PES and BP-PES are not crystallized, but they are in amorphous state. The main peaks (I) in Figure 2.4, around 2θ ~ 18° in both samples represent the nearest intermolecular distance (~ 4.9 Å) of CH_n–CH_n groups.[32] Unlike BP-PES showing a single broad amorphous halo peak, SBI-PES shows a characteristic shoulder (II) around 2θ ~ 13° that corresponds to the inter-distance (~6.8 Å) between the centers of the polymer backbone. The difference in chain thicknesses between the alternating thick spirobiindane unit and thin arylene ether sulfone unit makes the porous channel suitable for gas diffusion. The vertical pore dimension (~ 8 Å) was estimated from the correlation distance (4.9 Å) and the cross-sectional dimensions and the length (11.96 Å) of the arylene ether sulfone unit. A schematic view of the chain-chain correlation is shown in Figure 2.5. Since the pre-peak (II) appears as a shoulder rather than a well-defined peak shape, the inter-correlation distance between the main chains can have a broad distribution.

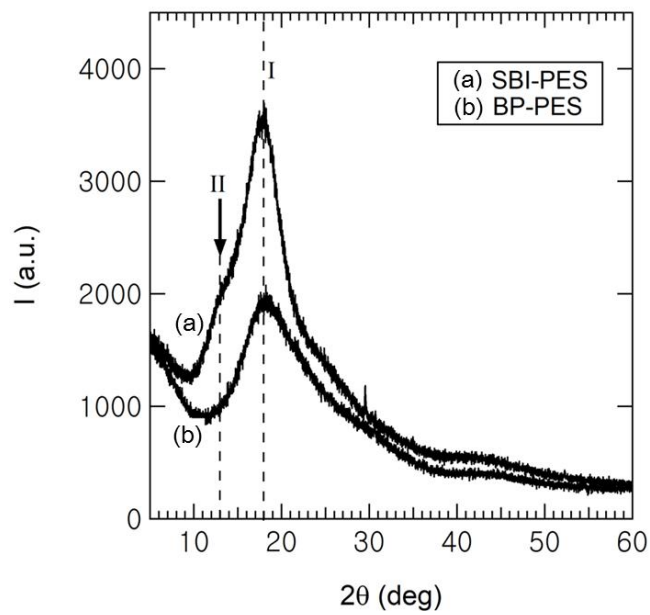

Figure 2.4 X-Ray diffraction spectra of a) SBI-PES and b) BP-PES. Arrow indicates a pre-peak representing a correlation distance between polymer main chains of SBI-PES (see schematic view).

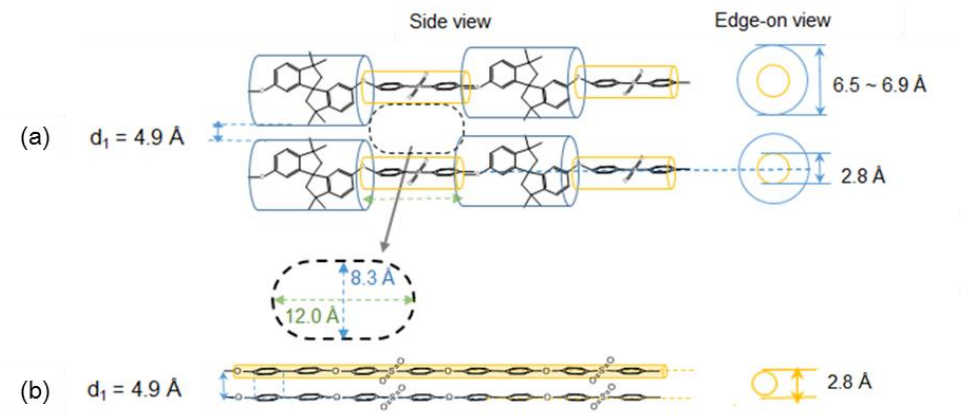

Figure 2.5 Schematic views of the correlation distances and cross-sections of a) SBI-PES and b) BP-PES measured from the XRD. The pore generated by the difference of chain thicknesses between two alternating chains. The vertical pore dimension was estimated from the correlation distance and cross-section dimensions and the horizontal dimension from the molecular dimension of arylene ether sulfone.

2.3.2. Synthesis and characterization of poly(arylene ether sulfone) containing quaternary ammonium hydroxide and spirobiindane groups (QOH-SBIs)

SBI-PES has better gas permeability. We introduced this concept in the electrode electrolyte binder in AEMFC MEA. One of the key requirements of the electrode binder for AEMFC MEA is its OH^- conducting ability. We used PES-containing quaternary ammonium hydroxide to conduct OH^- ions, as published previously.[5]

QIx-SBI(100-x)s (x means the molar ratio of the monomer unit, which has a quaternary ammonium pendant group in di-hydroxyl monomers) (Figure 2.2c) were obtained from the reaction of 2,5,2',5'-tetra(trimethylaminemethylene)-4,4'-dihydroxydiphenylether[33], spirobiindane bisphenol and 4,4'-difluorodiphenyl sulfone followed by the treatment of methyl iodide (Scheme 2.1). QIx-BP(100-x)s were also synthesized using biphenol instead of spirobiindane bisphenol by the same method. The polymer structures were confirmed and identified by ^1H NMR as shown in Figure 2.6. QIx-SBI(100-x)s and QIx-BP(100-x)s were converted to QOHx-SBI(100-x)s and QOHx-BP(100-x)s (OH^- conducting electrolytes) (Figure 2.2d) by KOH treatment. The degree of functionality (DF) values were measured from the peak area ratio of $-N^+-CH_3$ protons to aromatic protons in ^1H NMR (Table 2.4). The DF values well match the value intended for the polymerization. The DF values were used to calculate IEC_{NMR} values. IEC_{NMR} values were also similar to $IEC_{theoretical}$ values, confirming the synthesis.

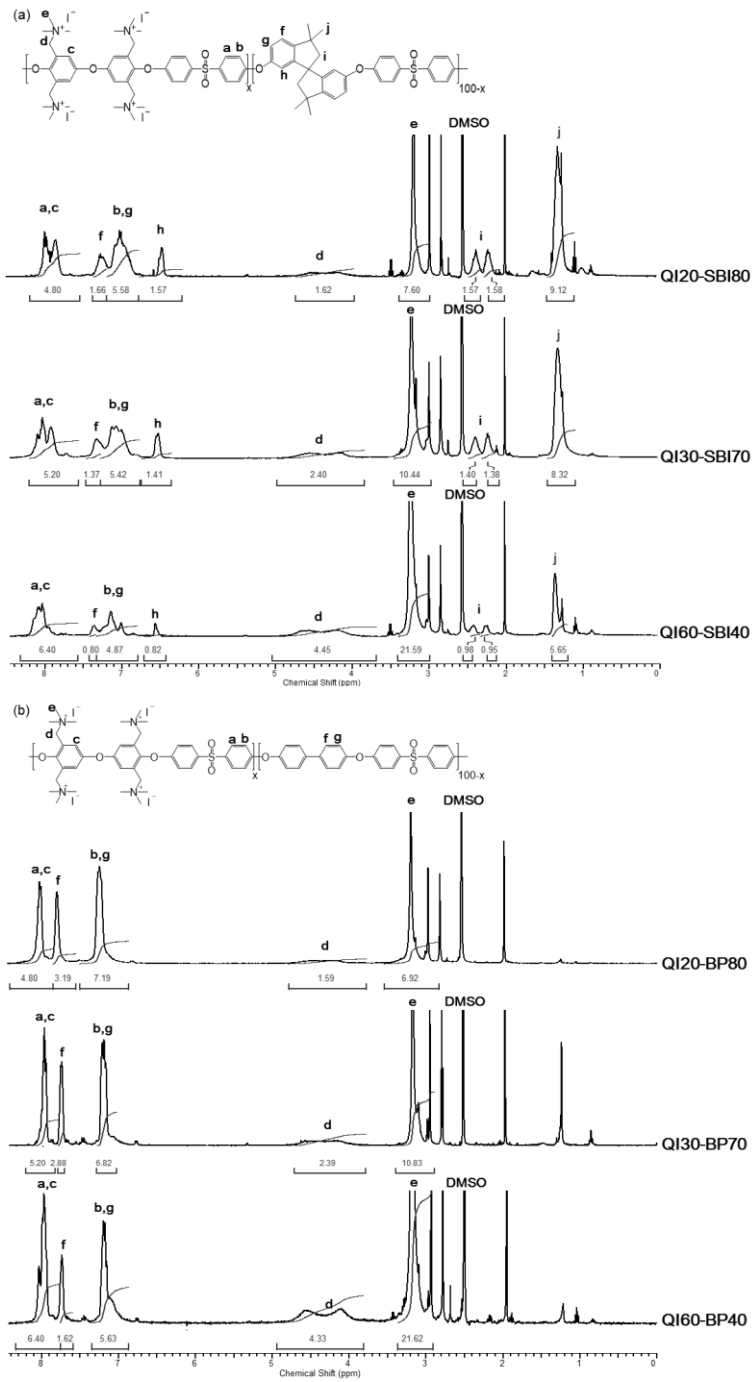

Figure 2.6 ^{1}H NMR spectra of PES containing quaternary ammonium iodide and a) spirobiindane group (QIx-SBI(100-x)s) and b) biphenyl group (QIx-BP(100-x)s).

Table 2.4 DF values and ion exchange capacity of QOHx-SBI(100-x)s and QOHx-BP(100-x)s electrolyte.

Sample	DF values	IEC_{NMR} (meq g^{-1})	$IEC_{theoretical}$ (meq g^{-1})	$IEC_{titration}$ (meq g^{-1})
QOH20-SBI80	20	1.40	1.40	1.05 ± 0.17
QOH30-SBI70	30	2.01	2.01	1.14 ± 0.13
QOH60-SBI40	56	3.38	3.57	1.80 ± 0.12
QOH20-BP80	20	1.68	1.68	1.09 ± 0.20
QOH30-BP70	30	2.34	2.34	1.18 ± 0.19
QOH60-BP40	54	3.59	3.85	1.97 ± 0.24

Table 2.5 Water uptake and conductivity of QOHx-SBI(100-x)s and QOHx-BP(100-x)s electrolyte.

Sample	Water uptake (%)				Conductivity (S cm^{-1})			
	30 °C	40 °C	60 °C	80 °C	30 °C	40 °C	60 °C	80 °C
QOH20-SBI80	7.4 ± 2.1	7.6 ± 2.5	8.0 ± 2.7	8.3 ± 2.9	0.019	0.022	0.024	0.024
QOH30-SBI70	10.2 ± 4.0	10.9 ± 2.3	11.8 ± 2.0	12.3 ± 2.2	-[a]	-[a]	-[a]	-[a]
QOH60-SBI40	503.2 ± 27.4	-[b]	-[b]	-[b]	-[a]	-[a]	-[a]	-[a]
QOH20-BP80	6.8 ± 1.6	7.0 ± 2.1	7.9 ± 2.2	8.6 ± 2.6	0.010	0.013	0.017	0.022
QOH30-BP70	12.6 ± 1.5	13.1 ± 1.9	15.3 ± 1.7	16.7 ± 1.8	0.016	0.017	0.022	0.027
QOH60-BP40	-[a]	-[b]	-[b]	-[b]	-[a]	-[a]	-[a]	-[a]

[a] Membranes were too brittle to measure the properties.
[b] It was dissolved in water.

The water uptake is related to OH^- conducting properties. Generally, the more water uptake, the higher the OH^- conductivity. The water uptake values increased with the content of the quaternary ammonium moieties (high DF value). In case of equal DF values, IEC values of QOHx-SBI(100-x)s were lower than that of QOHx-BP(100-x)s but their water uptake were similar. The bulky structure of the spirobiindane unit generates larger inter-chain pores that can absorb more water.

The TGA and DTG profiles show the thermal stability of the polymers. In the thermograms of SBI-PES and BP-PES, the weight loss from 400 °C to 650 °C could be attributed to the degradation of the polymer's main-chain (Figure 2.7a). The series of QOHx-SBI(100-x)s and QOHx-BP(100-x)s had two thermal degradation steps. The decomposition of quaternary ammonium hydroxide appeared at the first loss from 150 °C, and the degradation of the polymer main-chain appeared at the second loss up to 650 °C (Figure 2.7b).

The FTIR analysis was used to characterize chemical bonds and identify functional group of materials (Figure 2.8). 1587 cm^{-1} peak is related to aromatic C-C stretching and 1149 cm^{-1} is characteristic peak of O-S-O stretching, respectively. 831 cm^{-1} and 941 cm^{-1} peaks are due to C-H stretching of aromatic rings. C-N stretching of quaternary ammonium peak appeared at 670 cm^{-1}.

The alkaline stability test of ionomers was performed by immersing the membranes in 2 M NaOH at 80 °C for 24 h. The samples were washed and dissolved in DMSO-d_6 to obtain ^1H NMR spectrum. In Figure 2.9, there were the peak area ratio decrease of the quaternary ammonium protons (3.2 ppm) to the

aromatic protons (6.3–8.3 ppm) as the alkaline degradation of PES containing quaternary ammonium has been reported.[34, 35]

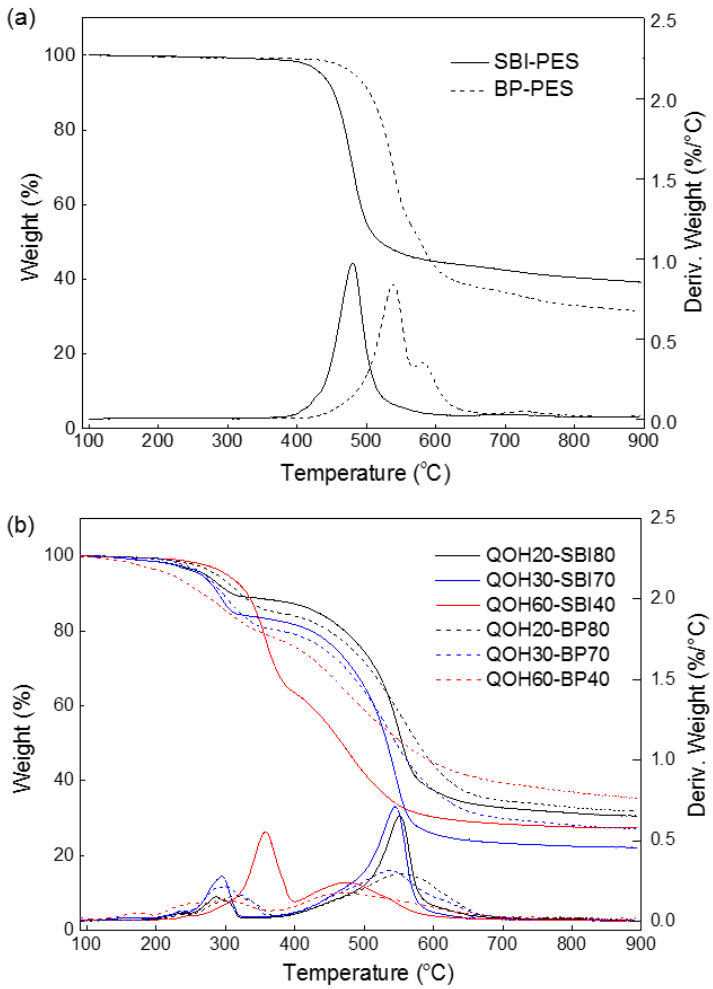

Figure 2.7 The TGA and DTG profiles of a) SBI-PES and BP-PES, b) QOHx-SBI(100-x)s and QOHx-BP(100-x)s.

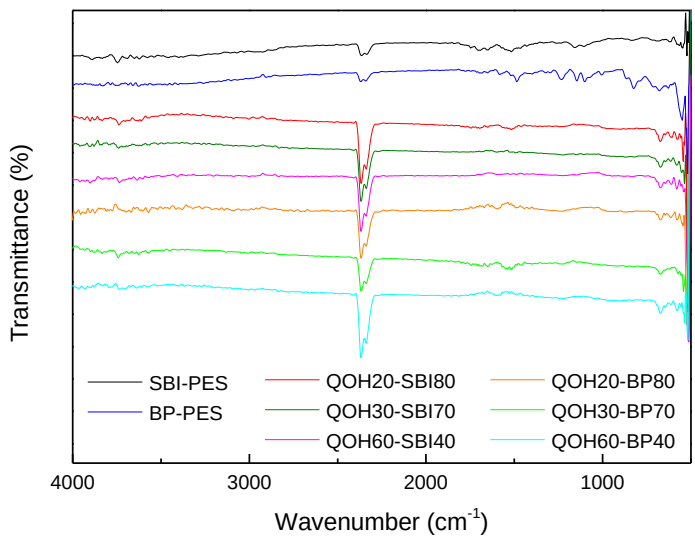

Figure 2.8 FT-IR results of synthetic polymers.

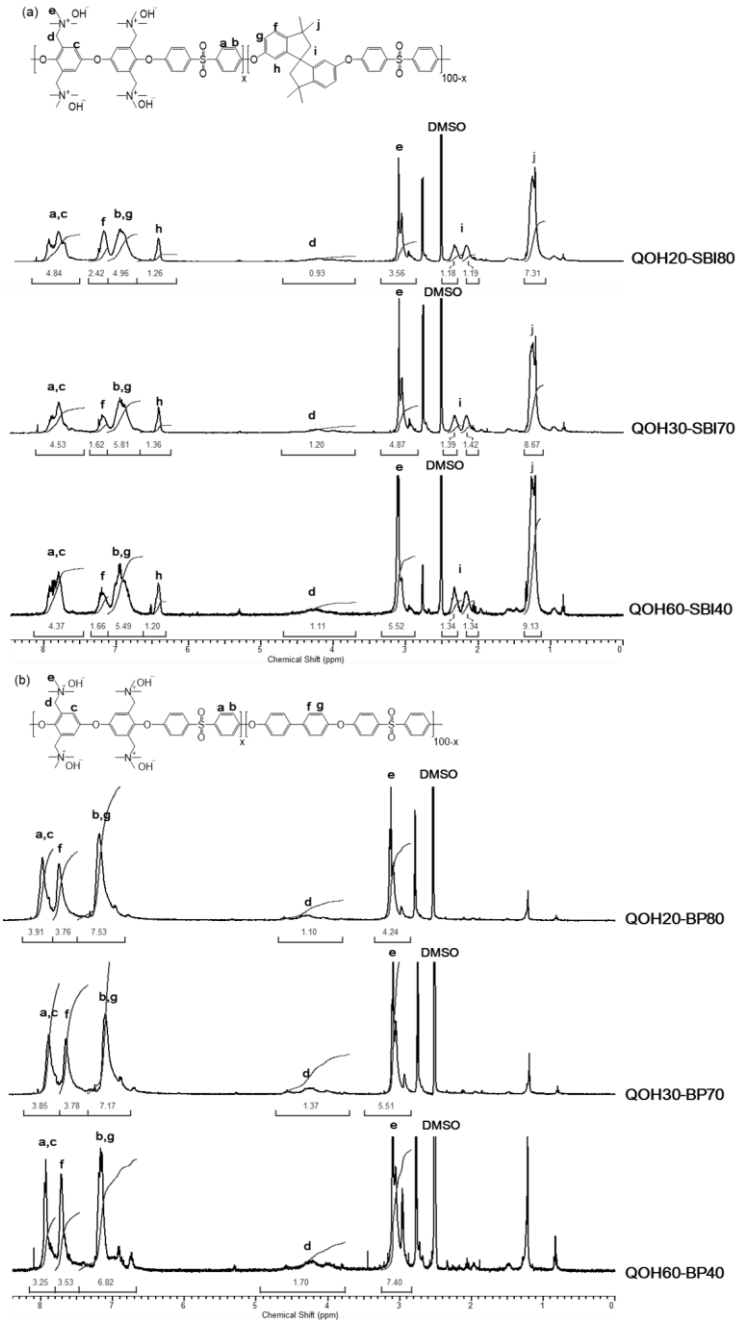

Figure 2.9 ^{1}H NMR spectra change of PES containing quaternary ammonium hydroxide and a) spirobiindane group (QIx-SBI(100-x)s) and b) biphenyl group (QIx-BP(100-x)s) immersed in 2 M NaOH at 80 ^{o}C for 24 h.

2.3.3. Chain conformation of QOH-SBI in solution

QOH-SBIs were too brittle for gas permeability measurement unlike SBI-PES (Table 2.5). Therefore, we investigated the structural characteristics of QOH-SBI in solution to investigate chain rigidity, using the SANS measurement. Figure 2.10 shows the SANS profiles of QOH30-SBI70 and QOH30-BP70 measured at 25 °C. Below Q ~ 0.02 $Å^{-1}$, QOH30-SBI70 shows a strong low-angle scattering while QOH30-BP70 shows trivial weak (or negligible) scattering. The strong low angle upturn indicates that QOH30-SBI70 polymers in the DMSO-d_6 solvent aggregated while QOH30-BP70 was well dispersed to show only a single chain conformation without interacting with each other. The difference in solubility (i.e., DMSO-d_6 is a good solvent for QOH30-BP70 and poor solvent for QOH30-SBI70) can be a reason for this phenomenon. The aggregated QOH30-SBI70 chains dissociate with the decrease in low-angle scattering at Q < 0.01 $Å^{-1}$ and an increase in temperature from 25 °C (closed triangle) to 70 °C (open triangle), suggesting that the solubility increases at high temperature.

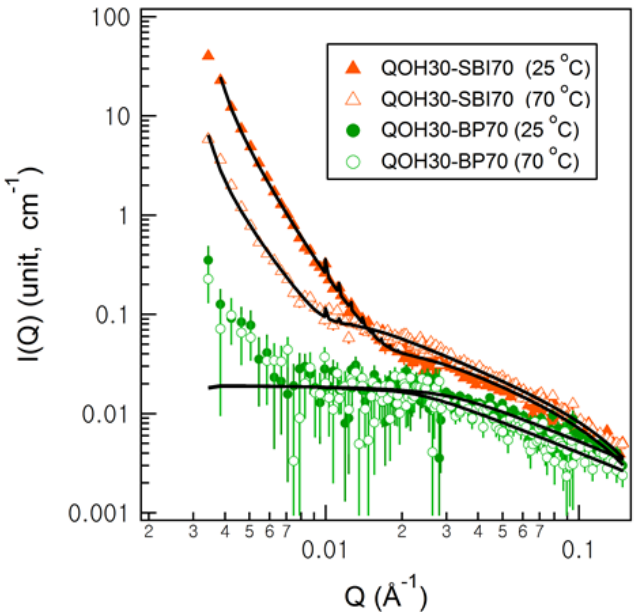

Figure 2.10 SANS profiles of QOH30-SBI70 and QOH30-BP70 at 25 °C (closed symbol) and 70 °C (open symbol). The incoherent scattering was removed. Solid lines are the fits from the worm-like chain model with a power law scattering.

The chain stiffness of the samples, QOH30-SBI70 and QOH30-BP70, was investigated using the worm-like chain including the excluded volume expressed as

$$I(Q) \sim k(\Delta SLD)^2 S(Q, L_k, l_k) P_{cs}(Q, R) \quad (12)$$

where k is a scale factor, ΔSLD is the difference in scattering length density between the polymer and the solvent, $S(Q,L_c,l_k)$ is the scattering function of the single semi-flexible chain with an excluded volume effect, and $P_{cs}(Q,R)$ is the form factor of the cross-section of a rod-like shape. The L_c,l_k, R are the contour length, Kuhn length, and cross-sectional radius, respectively. The details of each scattering function in Equation (12) are well described in the references[36, 37]. The schematic SANS profiles of the worm-like model are shown in Figure 2.11. The three characteristic features are, low Q (region 1), intermediate Q (region 2), and high Q (region 3) areas. The low Q region (region 1) is related to the radius of gyration.

$$R_g^2 \sim \frac{L_c l_k}{6} \quad (13)$$

Region 2 represents a rod-like shape with a typical slope of -1 and the transition between region 1 and region 2 represents the Kuhn length that is somewhat interfered by the contour length. Region 3 represents the cross-sectional radius of the chain that is the most reliable dimension in the fitting since the effect of the low Q scattering is negligibly small. In addition, when the chains aggregate (for example, in a poor solvent), the aggregates cause a power law scattering at low Q (similar to region 1), representing the large structure.

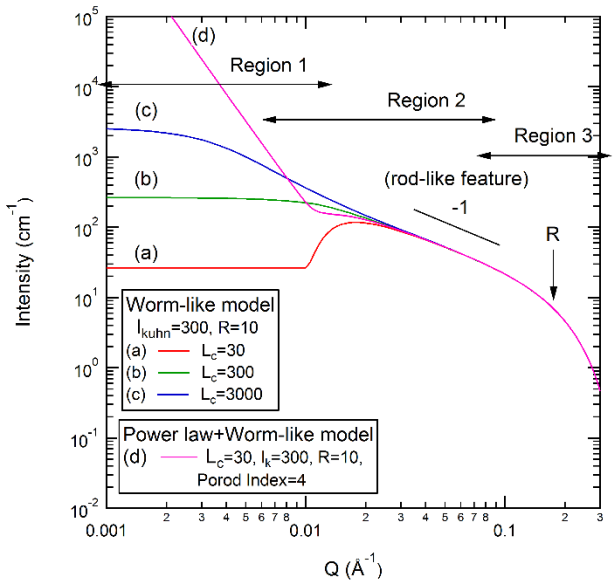

Figure 2.11 Calculated SANS profiles (*I* versus *Q* plot) of the worm-like chain with different contour length, Kuhn length, and cross-sectional radius, adding the power law model.

By adding power law scattering to Equation (12), where *m* is a power law index and k_p is a constant, Fig. 2.11d is obtained.

$$I_p\ (Q) \sim k_p\ Q^{-m} \qquad (14)$$

In this case, it is somewhat difficult to obtain a reliable contour length and Kuhn length owing to the strong interference by the power law scattering while *R* is still reliable. Thus, care must be exercised when fitting the data to the model. Overall, the scattering profiles of QOH30-SBI70 and QOH30-BP70 in the DMSO-d_6 solvent approximately match Figure 2.11c and Figure 2.11d, respectively.

The average cross-sectional diameters (*D*) of two copolymers, QOH30-SBI70 and QOH30-BP70, at two different temperatures, 25 °C and 70 °C, are shown in Table 2.6. The chain diameter of QOH30-SBI70 containing quaternary ammonium moieties and spirobiindane groups on the chain backbone is 22–23 Å, approximately four times the diameter (5 Å) of QOH30-BP70 containing quaternary ammonium moieties and diphenyl ether units on the chain backbone. Temperature does not significantly affect the cross-sectional diameter of the chain as expected. The larger diameter can be explained by the greater bulkiness of the spirobiindane group compared to the diphenyl ether group.

Table 2.6 SANS characterizations using the worm-like chain model of QOH30-SBI70 and the QOH30-BP70 in DMSO-d_6 solvent at 25 °C and 70 °C[a)]

Sample	T (°C)	D (Å)	l_k[b)] (Å)	L_c (Å)
QOH30-SBI70	25	23 ± 2	188 ± 6	60 ± 5
	70	22 ± 1	348 ± 1	33 ± 15
QOH30-BP70	25	5 ± 4	123 ± 72	112 ± 25
	70	5 ± 5	198 ± 140	148 ± 73

a) Uncertainties are one standard deviation (68% confidence level).
b) $l_k = 2l_p$, where l_p is called the persistence length by Porod since l_k (or l_p) characterize the chain stiffness.[38]

The Kuhn length (i.e., the statistical segment length) of QOH30-SBI70 is larger than that of QOH30-BP70 at the same temperature. The larger size in both the diameter and the statistical segment length indicates that QOH30-SBI70 is stiffer than QOH30-BP70 because of the incorporation of the bulky spirobiindane group in the backbone that restricts the rotation of the chain segment while the phenyl in the spirobiindane-free QOH30-BP70 can rotate so that the chain is more flexible as shown in the chemical structure of the chains (see Figure 2.2). The Kuhn length in the semi-flexible chain increases with temperature in both polymers because increasing temperature enhances solubility. Thus, the expanding chain increases the Kuhn length. For example, from l_k = 188 Å at 25 °C to l_k = 348 Å at 70 °C for QOH30-SBI70 and l_k = 123 Å at 25 °C to l_k = 198 Å at 70 °C for QOH30-BP70.

When the stiffness of the polymer is coupled with increases in inter-chain spacing, its permeability is enhanced.[39, 40] According to WAXD analysis, spirobiindane modified PES has wider inter-chain distance than pristine PES. As mentioned above, QOH30-SBI70 is stiffer than QOH30-BP70. These two measurements explain why QOH30-SBI70 has high gas permeability.

2.3.4. Anion exchange membrane fuel cell (AEMFC) performance of QOHx-SBI(100-x)s

The highly gas permeable QOH-SBI is evaluated for its practical application in the electrode of a fuel cell. QOHx-SBI(100-x)s and QOHx-BP(100-x)s were used, respectively, as electrode binders in AEMFC MEA. Figure 2.12 shows the effects of the spirobiindane unit of the electrolyte binders on AEMFC. QOHx-SBI(100-x)s show higher current density than their analogs, QOHx-BP(100-x)s. Assuming that QOHx-SBI(100-x)s and QOHx-BP(100-x)s have the same DF for the same x, bulky spirobiindane unit plays a significant role in increasing the cell performance by enhancing gas permeability.

Three QOHx-SBI(100-x)s, which have different molar ratios of quaternary ammonium moieties and spirobiindane units, were synthesized. A larger number of quaternary ammonium moieties increase the water uptake and thus OH^- conductivity. The more spirobiindane units, the higher the gas permeability, and the higher the cell performance. However, we could not simultaneously synthesize the polymers that have these two groups, because the monomers, 2,5,2',5'-tetra(trimethylaminemethylene)-4,4'-dihydroxydiphenylether (TADHDPE) for high water uptake and spirobiindane bisphenol (SBI) for high gas permeability, have di-hydroxyl functionality. Therefore, when one property is increased, the other is decreased.

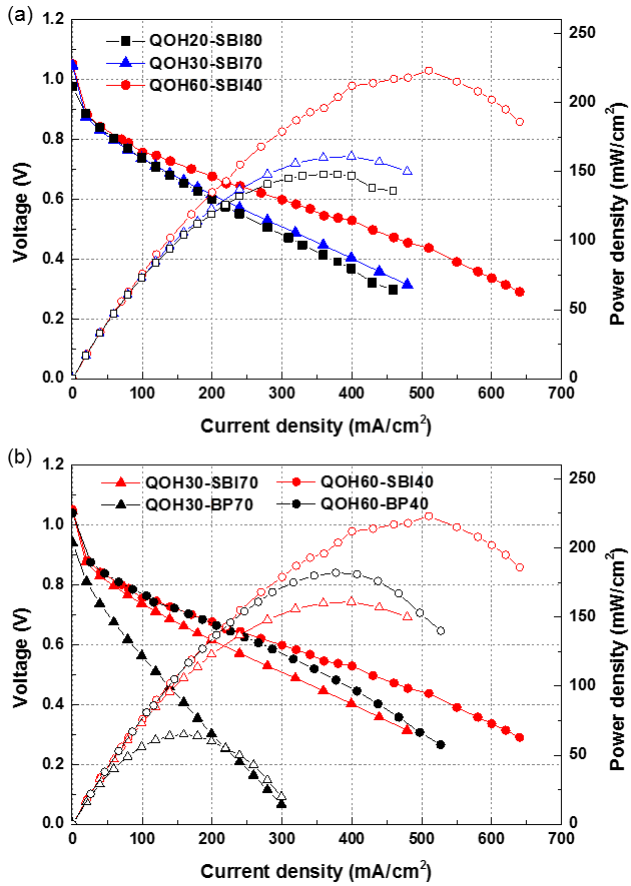

Figure 2.12 Polarization and power density curves of H_2/O_2 AEMFCs employing (a) QOHx-SBI(100-x)s and (b) QOHx-BP(100-x)s.

There is a slight difference in cell performance of QOH20-SBI80 and QOH30-SBI70. Even though QOH30-SBI70 shows better cell performance than QOH20-SBI80, the improvement is about 10% at 0.6 V. Compared to QOH20-SBI80 and QOH30-SBI70, QOH60-SBI40 showed a considerably high cell performance. The MEA with spirobiindane-modified PES shows 1.2 times higher maximum power density than that of spirobiindane-free PES. A MEA using QOH60-SBI40 achieved a peak power density of 223 mW cm^{-2} and current density of 280 mA cm^{-2} at 0.6 V.

In Table 2.5, the water uptake of QOH20-SBI80 and QOH30-SBI70 were on a similar level but QOH60-SBI40 absorbed 500% more water because of the high degree of ammonium hydroxyl functionality. Thus, small changes in the molar ratio of two monomers, TADHDPE and spirobiindane bisphenol, do not have a significant influence on the cell performance. In addition, high water uptake of QOH60-SBI40 increases its gas permeability although the portion of the spirobiindane unit in QOH60-SBI40 is lower than that in QOH20-SBI80 and QOH30-SBI70. According to previous studies, the gas permeability of polymer electrolyte increases with relative humidity.[41, 42] Therefore, the high cell performance of QOH60-SBI40 is caused by high water uptake of the electrolyte, as well as its high gas permeability. Our experiments show that both water uptake and gas permeability are key characteristics of the electrode binding materials of MEA of AEMFC. We could not analyze the dimensional changes in QOH60-SBI40 because of its fragility. It is very difficult to measure the dimensional changes in powder-like electrolytes. The dimensional stability of the binder is also important

for the MEA. Future studies will focus on the enhancement of water uptake and gas permeability with the low dimensional change of the binder.

2.4. Conclusions

The results of this study confirm that the presence of spirobiindane moieties in polymer backbone helps increase gas permeability and AEMFC performance. Our results are the first reported data on the numerical dimension of bulky moieties in main-chain and also its performance for AEMFCs. Compared with the common poly(arylene ether sulfone) (PES), the spirobiindane-based PES shows high gas permeability caused by the increased fractional free volume. We suggest that the difference in chain thicknesses between the alternating thick SBI unit and thin PES unit makes the microporous channel suitable for gas diffusion and water uptake. As a result of characterization of a synthetic polymer series, PES containing spirobiindane moiety and tetra(quaternary ammonium) pendant groups as AEMFC electrode binders, both adequate water uptake and high gas permeability of the electrode binder contribute to the cell performance improvement. PES containing tetra(quaternary ammonium) hydroxide and spirobiindane group is a good candidate as an electrode binding material for AEMFCs.

2.5. References

[1] H.-J. Kim, Single cell for proton exchange membrane fuel cells (PEMFCs), in: D. Stolten, R. C. Samsun, N. Garland (Eds.), Fuel Cells: Data, Facts, and Figures, Wiley-VCH: Weinheim (2016), pp. 135-140.

[2] J. Catalano, T. Myezwa, M.G. De Angelis, M.G. Baschetti, G.C. Sarti, The effect of relative humidity on the gas permeability and swelling in PFSI membranes, *Int. J. Hydrogen Energy* (2012), **37**, 6308-6316.

[3] G. Sasikumar, J.W. Ihm, H. Ryu, Dependence of optimum Nafion content in catalyst layer on platinum loading, *J. Power Sources* (2004), **132**, 11-17.

[4] Y. Kwon, S.Y. Lee, S. Hong, J.H. Jang, D. Henkensmeier, S.J. Yoo, H.-J. Kim, S.-H. Kim, Novel sulfonated poly(arylene ether sulfone) containing hydroxyl groups for enhanced proton exchange membrane properties, *Polym. Chem.* (2015), **6**, 233-239.

[5] J. Choi, Y.-J. Byun, S.Y. Lee, J.H. Jang, D. Henkensmeier, S.J. Yoo, S.-A. Hong, H.-J. Kim, Y.-E. Sung, J.-S. Park, Poly(arylene ether sulfone) with tetra(quaternary ammonium) moiety in the polymer repeating unit for application in solid alkaline exchange membrane fuel cells, *Int. J. Hydrogen Energy* (2014), **39**, 21223-21230.

[6] H.-J. Lee, Y. Kwon, S.Y. Lee, J. Choi, B.H. Kim, D. Henkensmeier, J.H. Jang, S.J. Yoo, J.-Y. Kim, H.-J. Kim, H. Kim, M.-H. Kim, Facile preparation of a long-term durable nano- and micro-structured polymer

blend membrane for a proton exchange membrane fuel cell, *RSC Adv.* (2016), **6**, 46516-46522.

[7] N.N. Krishnan, H.-J. Kim, J.H. Jang, S.-Y. Lee, E. Cho, I.-H. Oh, S.-A. Hong, T.-H. Lim, Sulfonated poly(ether sulfone)-based catalyst binder for a proton-exchange membrane fuel cell, *J. Appl. Polym. Sci.* (2009), **113**, 2499-2506.

[8] L.M. Robeson, The upper bound revisited, *J. Membr. Sci.* (2008), **320**, 390-400.

[9] X. Ma, O. Salinas, E. Litwiller, I. Pinnau, Pristine and thermally-rearranged gas separation membranes from novel o-hydroxyl-functionalized spirobifluorene-based polyimides, *Polym. Chem.* (2014), **5**, 6914-6922.

[10] T. Kaneko, K. Yamamoto, M. Asano, M. Teraguchi, T. Aoki, Synthesis of poly(phenylacetylene)-based polydendrons consisting of a phenyleneethynylene repeating unit, and oxygen/nitrogen permeation behavior of their membranes, *J. Membr. Sci.* (2006), **278**, 365-372.

[11] Y.J. Cho, H.B. Park, High performance polyimide with high internal free volume elements, *Macromol. Rapid Commun.* (2011), **32**, 579-586.

[12] S.K. Sen, S. Banerjee, Spiro-biindane containing fluorinated poly(ether imide)s: Synthesis, characterization and gas separation properties, *J. Membr. Sci.* (2010), **365**, 329-340.

[13] D. Guzmán-Lucero, J. Palomeque-Santiago, C. Camacho-Zúñiga, F. Ruiz-Treviño, J. Guzmán, A. Galicia-Aguilar, C. Aguilar-Lugo, Gas permeation

properties of soluble aromatic polyimides based on 4-fluoro-4,4'-diaminotriphenylmethane, *Materials* (2015), **8**, 1951-1965.

[14] G. Chen, X. Zhang, S. Zhang, T. Chen, Y. Wu, Synthesis, properties, and gas permeation performance of cardo poly(arylene ether sulfone)s containing phthalimide side groups, *J. Appl. Polym. Sci.* (2007), **106**, 2808-2816.

[15] J.E. Chae, B.H. Kim, J.H. Noh, J. Jung, J.-Y. Kim, J.H. Jang, S.J. Yoo, H.-J. Kim, S.Y. Lee, Effect of the spirobiindane group in sulfonated poly(arylene ether sulfone) copolymer as electrode binder for polymer electrolyte membrane fuel cells, *J. Ind. Eng. Chem.* (2017), **47**, 315-322.

[16] S. Sambandam, J. Parrondo, V. Ramani, Estimation of electrode ionomer oxygen permeability and ionomer-phase oxygen transport resistance in polymer electrolyte fuel cells, *Phys. Chem. Chem. Phys.* (2013), **15**, 14994-15002.

[17] R. Shimizu, Y.-C. Park, K. Kakinuma, A. Iiyama, M. Uchida, Effects of both oxygen permeability and ion exchange capacity for cathode ionomers on the performance and durability of polymer electrolyte fuel cells, *J. Electrochem. Soc.* (2018), **165**, F3063-F3071.

[18] I. Kruusenberg, L. Matisen, Q. Shah, A.M. Kannan, K. Tammeveski, Non-platinum cathode catalysts for alkaline membrane fuel cells, *Int. J. Hydrogen Energy* (2012), **37**, 4406-4412.

[19] D.R. Dekel, Review of cell performance in anion exchange membrane fuel cells, *J. Power Sources* (2018), **375**, 158-169.

[20] S. Gottesfeld, D.R. Dekel, M. Page, C. Bae, Y. Yan, P. Zelenay, Y.S. Kim, Anion exchange membrane fuel cells: current status and remaining challenges, *J. Power Sources* (2018), **375**, 170-184.

[21] L. Wang, E. Magliocca, E.L. Cunningham, W.E. Mustain, S.D. Poynton, R. Escudero-Cid, M.M. Nasef, J. Ponce-González, R. Bance-Souahli, R.C.T. Slade, D.K. Whelligan, J.R. Varcoe, An optimised synthesis of high performance radiation-grafted anion-exchange membranes, *Green Chem.* (2017), **19**, 831-843.

[22] M.-S. Shin, Y.-J. Byun, Y.-W. Choi, M.-S. Kang, J.-S. Park, On-site crosslinked quaternized poly(vinyl alcohol) as ionomer binder for solid alkaline fuel cells, *Int. J. Hydrogen Energy* (2014), **39**, 16556-16561.

[23] S.D. Poynton, R.C.T. Slade, T.J. Omasta, W.E. Mustain, R. Escudero-Cid, P. Ocón, J.R. Varcoe, Preparation of radiation-grafted powders for use as anion exchange ionomers in alkaline polymer electrolyte fuel cells, *J. Mater. Chem. A* (2014), **2**, 5124-5130.

[24] D. Yang, H. Yu, G. Li, Y. Zhao, Y. Liu, C. Zhang, W. Song, Z. Shao, Fine microstructure of high performance electrode in alkaline anion exchange membrane fuel cells, *J. Power Sources* (2014), **267**, 39-47.

[25] X. Gao, H. Yu, J. Jia, J. Hao, F. Xie, J. Chi, B. Qin, L. Fu, W. Song, Z. Shao, High performance anion exchange ionomer for anion exchange membrane fuel cells, *RSC Advances* (2017), **7**, 19153-19161.

[26] J.G. Seong, Y. Zhuang, S. Kim, Y.S. Do, W.H. Lee, M.D. Guiver, Y.M. Lee, Effect of methanol treatment on gas sorption and transport behavior of

intrinsically microporous polyimide membranes incorporating Tröger′s base, *J. Membr. Sci.* (2015), **480**, 104-114.

[27] W.-H. Lee, Y.S. Kim, C. Bae, Robust hydroxide ion conducting poly(biphenyl alkylene)s for alkaline fuel cell membranes, *ACS Macro Lett.* (2015), **4**, 814-818.

[28] S.R. Kline, Reduction and analysis of SANS and USANS data using IGOR Pro, *J. Appl. Cryst.* (2006), **39**, 895-900.

[29] J. Wang, J. Wang, S. Li, S. Zhang, Poly(arylene ether sulfone)s ionomers with pendant quaternary ammonium groups for alkaline anion exchange membranes: Preparation and stability issues, *J. Membr. Sci.* (2011), **368**, 246-253.

[30] W.-F. Chen, H.-Y. Lin, S.A. Dai, Generation and synthetic uses of stable 4-[2-isopropylidene]-phenol carbocation from bisphenol A, *Org. Lett.* (2004), **6**, 2341-2343.

[31] J.Y. Han, J.Y. Lee, H.-J. Kim, M.-H. Kim, S.G. Han, J.H. Jang, E.A. Cho, S.J. Yoo, D. Henkensmeier, Synthesis and characterization of fluorene-based polybenzimidazole copolymer for gas separation, *J. Appl. Polym. Sci.* (2014), **131**, 40521-40529.

[32] M.-H. Kim, J.D. Londono, A. Habenschuss, Structure of molten stereoregular polyolefins with different sde-chain sizes: linear polyethylene, polypropylene, poly(1-butene), and poly(4-methyl-1-pentene), *J. Polym. Sci. B Polym. Phys.* (2000), **38**, 2480-2485.

[33] Y. Song, T. Tian, P. Wang, H. He, W. Liu, X. Zhou, X. Cao, X.L. Zhang, X. Zhou, Phenol quaternary ammonium derivatives: charge and linker effect on their DNA photo-inducible cross-linking abilities, *Org. Biomol. Chem.* (2006), **4**, 3358-3366.

[34] S. Miyanishi, T. Yamaguchi, Ether cleavage-triggered degradation of benzyl alkylammonium cations for polyethersulfone anion exchange membranes, *Phys. Chem. Chem. Phys.* (2016), **18**, 12009-12023.

[35] C.G. Arges, V. Ramani, Two-dimensional NMR spectroscopy reveals cation-triggered backbone degradation in polysulfone-based anion exchange membranes, *Proc. Natl. Acad. Sci. U. S. A.* (2013), **110**, 2490–2495.

[36] W.-R. Chen, P.D. Butler, Linda J. Magid, Incorporating intermicellar interactions in the fitting of SANS data from cationic wormlike micelles, *Langmuir* (2006), **22**, 6539-6548.

[37] J.S. Pedersen, P. Schurtenberger, Scattering functions of semiflexible polymers with and without excluded volume effects, *Macromolecules* (1996), **29**, 7602-7612.

[38] H. Benoit, P. Doty, Light scattering from non-Gaussian chains, *J. Phys. Chem.* (1953), **57**, 958–963.

[39] B.D. Freeman, Basis of permeability/selectivity tradeoff relations in polymeric gas separation membranes, *Macromolecules* (1999), **32**, 375–380.

[40] M.D. Guiver, Y.M. Lee, Polymer rigidity improves microporous membranes, *Science* (2013), **339**, 284-285.

[41] S.S. Kocha, J. Deliang Yang, J.S. Yi, Characterization of gas crossover and its implications in PEM fuel cells, *AlChE J.* (2006), **52**, 1916-1925.

[42] C.W. James, A. Roy, J.E. McGrath, E. Marand, Determination of the effect of temperature and humidity on the O_2 sorption in sulfonated poly(arylene ether sulfone) membranes, *J. Membr. Sci.* (2008), **309**, 141-145.

Chapter 3. Spirobiindane-based poly(arylene ether sulfone) ionomers with quarternary ammonium-functionalized alkyloxy side chain in alkaline anion exchange membrane fuel cells

3.1. Background

Among various alternative energy sources, fuel cells are regarded as the most anticipated power source owing to their high efficiencies and power densities for stationary and mobile applications. Especially, proton exchange membrane fuel cells (PEMFCs) have the largest range of applications due to their fast start-up times and low operating temperatures.[1] However, the downsides of PEMFCs include the probability of high fuel crossover in the electrolyte membranes and high costs caused by noble metal catalysts. In this aspect, alkaline anion exchange membrane fuel cell (AEMFC) systems have the advantages of using non-noble metals due to faster electrode reaction kinetics for the oxygen reduction reaction under alkaline conditions, and the OH^- ion-conducting direction prevents fuel crossover.[2] The challenges in the AEMFC research field are their poor alkaline stability and low cell performance of current anion exchange membranes (AEMs).

For high alkaline stability and conductivity of AEMs, long alkyloxy chains have begun to be introduced as spacers or extenders.[3-6] Flexible ether-type spacers can improve the local mobility of ion groups, which facilitates the formation of hydrophilic/hydrophobic micro-phase separation morphologies and enhances conductivity [7, 8].

As another important key component of AEMFCs, AEMFC electrode ionomers (AEIs) have the same problems as AEMs [9, 10]. Although most studies have focused on AEMs, research on AEIs should be increased to improve fuel cell performance.

Previously, we introduced a new functional group (spirobiindane unit) into an OH^- conductive polymer electrolyte for AEIs. The spirobiindane moieties of the main-chain increase the fractional free volume and subsequently the gas permeability of the spirobiindane-based poly(arylene ether sulfone) (PES) compared with common PES. Thus, a higher cell performance was achieved by establishing the three-phase boundary efficiently.[11] The spiro-structure could therefore be considered suitable for AEIs due to the resulting relatively high gas permeable properties.[12]

In this work, we synthesized a series of spirobiindane-based poly(arylene ether sulfone) AEIs with different main-chain structures (Figure 3.1). This structures are expected to enhance gas utilization. To investigate the effects of poly(arylene ether sulfone)s with quaternary ammonium (QA)-functionalized side chains on cell performance, these ionomer series were synthesized and characterized by NMR and thermogravimetric analysis (TGA), and their chemical stability was studied.

We also fabricated a single-cell using the synthesized AEIs and evaluated their performance to confirm their applicability to AEMFCs.

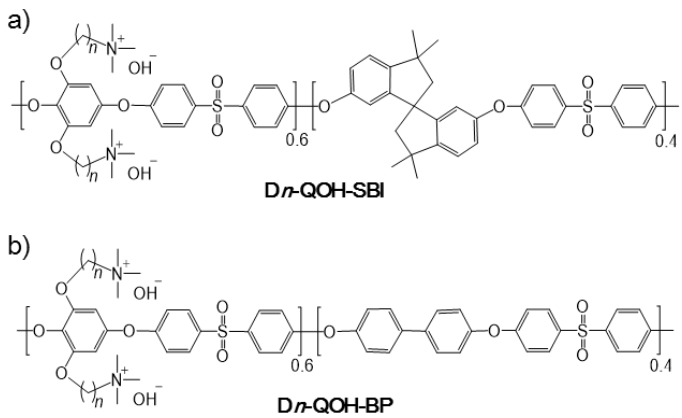

Figure 3.1 Molecular structures of poly(arylene ether sulfone) with QA-functionalized alkyloxy side chains. (D means "disubstituted". *n* is the alkyl chain length. Q represents quaternary ammonium and OH is hydroxide ion. SBI and BP refers to the spirobiindane and biphenyl, respectively.)

3.2. Experimental

3.2.1. Materials

4,4'-Difluorodiphenyl sulfone (DFDPS), 2,6-dimethoxyhydroxyquinone (DMHQ), 4,4'-biphenol, 1,6-dibromohexane, boron tribromide solution (1.0 M in DCM), trimethylamine solution (45 wt.% in H_2O), K_2CO_3, KI, anhydrous *N*-methyl-2-pyrrolidone (NMP), anhydrous toluene, anhydrous dimethylsulfoxide, anhydrous dichloromethane, and methanol were purchased from Sigma-Aldrich and used without additional purification. (2-Bromoethyl)trimethylammonium bromide was purchased from TCI chemicals, and methanol and isopropanol were purchased from Daejung and Honeywell, respectively. Previously synthesized spirobiindane bisphenol (SBIBP) was used.[11] Prior to synthesis, all monomers and polymers were dried overnight in a vacuum oven at 60 °C. For single-cell tests, FAA-3-50 AEMs and FAA-3 AEIs were purchased from Fumatech. The Pt/C electrocatalyst from Tanaka Kikinzoku Kogyo (K. K.) and gas diffusion layers (Sigracet® 39BC) from SGL Carbon were used in this study.

3.2.2. Characterization and methods

^{1}H NMR spectra were obtained using a Bruker 400 MHz AVANCE-III spectrometer with synthesized products dissolved in deuterated dimethylsulfoxide or chloroform. Two drops of trifluoroacetic acid were added to the NMR samples to prevent the water peak from overlapping with sample signals. Degree of

functionality (DF_{NMR}) values were determined from the peak area ratio of $–N^+–CH_3$ protons to aromatic protons in each ^1H NMR spectrum. Additionally, $IEC_{Theoretical}$ and IEC_{NMR} values were calculated from the estimated molecular weight of the repeat unit and DF_{Target} and DF_{NMR} values, respectively.

$$DF_{NMR} = \frac{\text{Peak area ratio of N-CH}_3}{\text{Peak area ratio of aromatic H}} \quad (1)$$

$$IEC_{Theoretical} = \frac{DF_{Target} \times 2 \text{ equiv.}}{DF_{Target} \times MW_{R.U.\ of\ QOH} + ((100 - DF_{Target}) \times MW_{R.U.\ of\ SBI\ or\ BP})} \quad (2)$$

$$IEC_{NMR} = \frac{DF_{NMR} \times 2 \text{ equiv.}}{DF_{NMR} \times MW_{R.U.\ of\ QOH} + ((100 - DF_{NMR}) \times MW_{R.U.\ of\ SBI\ or\ BP})} \quad (3)$$

The molecular weights and polydispersity index of the polymers were analyzed by gel permeation chromatography (Waters 2414 refractive index detector) using 0.05 M LiBr in NMP as an eluent. The analysis was conducted at 40 °C at a 1.0 mL min^{-1} flow rate. TGA was performed using a Q50 apparatus (TA Instruments). Under N_2 atmosphere, 3 mg of the polymer was heated at a rate of 10 °C min^{-1} to 900 °C.

3.2.3. Synthetic procedures

Synthesis of poly(arylene ether sulfone)s with methoxy groups and spirobiindane groups (DMe-SBI)

Poly(arylene ether sulfone)s with methoxy groups and spirobiindane groups were synthesized by condensation polymerization in a 250 mL round-bottom flask using a mechanical stirrer, Dean–Stark trap, condenser, and gas adapter (Scheme 3.1). The synthetic procedure for the DMe-SBI polymer was as follows: A 250 mL round-bottom flask was charged with 2.5782 g (15 mmol) of DMHQ, 3.1153 g (10 mmol) of SBIBP, 6.4205 g (25 mmol) of DFDPS, and 6.9174 g (50 mmol) of potassium carbonate. Then, 106 mL of NMP and toluene (NMP: toluene = 2:1 v/v) were added. The reaction mixture was refluxed at 140 °C for 4 h, and an azeotropic mixture of toluene and water was collected and removed through a Dean–Stark trap. The reaction temperature was slowly increased to 180 °C over 24 h. The resulting viscous solution was poured into 1 L of isopropanol and washed several times with deionized water. The obtained polymer was filtered and dried at 60 °C under vacuum for 24 h (yield: 86.1%). This polymerization procedure was also applied for the preparation of DMe-BP (yield: 96.7%).

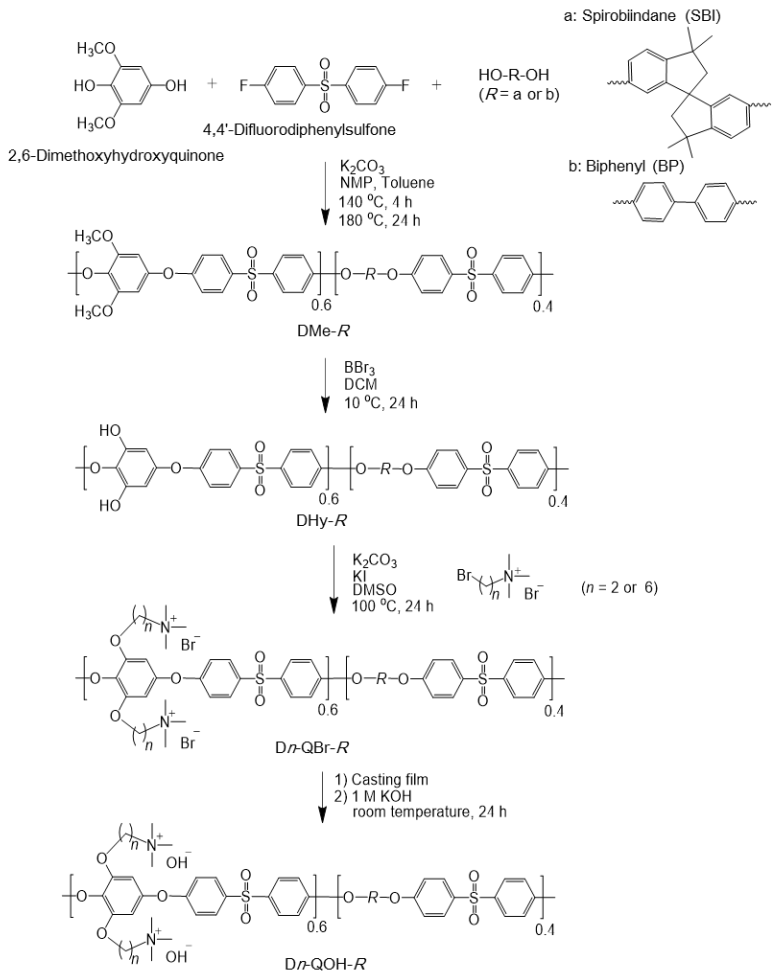

Scheme 3.1 Synthetic procedure of D*n*-QOH-SBIs and D*n*-QOH-BPs.

Conversion of methoxy groups of DMe-SBI to hydroxyl groups (DHy-SBI)

The methoxy groups were transformed into hydroxyl groups through a demethylation process according to the following steps: 8.0 g of DMe-SBI was dissolved in 240 mL of DCM in a 250 mL four-neck flask with an argon inlet. The reaction bath was cooled to 0 °C, and excess 1.0 M boron tribromide in DCM (20 mL) was injected dropwise into the reactor. The polymer was rapidly precipitated during this addition, and the reaction mixture was then stirred for a further 24 h. After the reaction, the polymer was filtered directly, washed with boiling water for 24 h, and dried at 60 °C under vacuum for 24 h (yield: 88.9%). This synthetic procedure was also applied for the preparation of DHy-BP (yield: 92.7%).

Synthesis of (6-bromohexyl)trimethylammonium bromide (Br-6-QA)

To a four-necked round-bottom flask equipped with a stirrer, condenser, thermometer, gas inlet, and pressure-equalizing dropping funnel, 46.09 mL (0.3 mol) of 45% trimethylamine solution and 210 mL of methanol were added and stirred, followed by dropwise addition of 48.07 mL (0.3 mol) of 1,6-dibromohexane over a 30-min period. The reaction mixture was allowed to stir at 25 °C for 4 h.[13] The resulting light-yellow solution was transferred to a round-bottom flask, and the solvent was removed under reduced pressure. The product was then purified by recrystallization with ethanol. The buff solid was dried under reduced pressure at 80 °C for 24 h (yield: 71.1%). [^{1}H NMR (DMSO-d_6, δ): 1.27-

1.49 (br, 4H), 1.60-1.92 (br, 4H), 3.03-3.12 (br, 9H), 3.26-3.33 (br, 2H), 3.41-3.69 (br, 2H)].

Synthesis of QA-functionalized DHex-QBr-SBI

DHy-SBI (3 g, 7.09 mmol –OH), K_2CO_3 (1.9807 g, 14.19 mmol), KI (0.3409 g, 2.04 mmol), and DMSO (60 mL) were added into a four-neck 100 mL round-bottom flask equipped with a magnetic stirrer, condenser, gas inlet, and thermometer. The mixture was heated to 100 °C for 6 h with stirring. Then, Br-6-QA (3.6902 g, 10.22 mmol) was added, and the reaction was continued at 100 °C for 24 h. After cooling the solution, the polymer was precipitated in isopropanol and washed with isopropanol and water several times. A brown powder was obtained after vacuum drying at 60 °C for 24 h (yield: 91.6%). This synthetic procedure was also applied for the preparation of DEth-QBr-SBI (yield: 88.4%), DEth-QBr-BP (yield: 73.6%), and DHex-QBr-BP (yield: 84.2%).

Counter-ion exchange from bromide form to hydroxide form

D*n*-QBr-SBIs (1 g) was dissolved in NMP (20 mL) to prepare a 5 wt% solution. The solution was filtered by using a 0.45 μm PTFE syringe filter and then cast onto glass dishes. After vacuum drying at 80 °C for 48 h, D*n*-QBr-SBIs were obtained in the form of fragments. To convert the polymer Br^- form into the OH^- form, the fragments were immersed in a 1 M KOH solution at room temperature for 24 h and then washed with DI water several times. D*n*-QOH-BPs were prepared in the same manner.

3.2.4. Alkaline stability test

Alkaline stabilities were examined by immersing the samples into a 0.1 M aqueous KOH solution at 60 °C for 170 h and 670 h. At the selected time, the membrane samples were rinsed by DI water repeatedly. Then, ^{1}H NMR spectra of the membranes were recorded.

3.2.5 Fuel-cell tests of MEAs

To prepare binder solution, the polymers were dissolved in DMAc (5 wt%), and the polymer solutions were filtered by using 0.45-μm PTFE cartridges.

Then, the catalyst slurry for the electrodes was prepared by dispersing 46.5 wt% Pt/C electrocatalyst (10.8 mg) in the binder solution (115.8 mg) and isopropanol (3.0 mL). This catalyst slurry was coated on both sides on the FAA-3-50 (Fumatech) by a spraying method. The area of a square was 5 cm^2. The Pt loading amount was 0.4 mg cm^{-2} on each side of the electrode, and the ionomer content was 35 wt%. A single-cell was assembled by a torque wrench at 70 kgf cm^{-2}.

The 5-cm^2 single-cell consisting of an MEA was operated at 60 °C and 100% RH. H_2 and O_2 gases were fed to the anode and cathode at flow rates both 200 mL min^{-1}. A single-cell was activated at 0.4 V using constant voltage mode for reaching steady-state. After a steady-state was reached, the cell was tested from OCV to 0.25 V for *I–V* polarization curves.

3.3. Results and discussion

3.3.1. Synthesis and characterization of Dn-QOH-SBIs and Dn-QOH-BPs

Poly(arylene ether sulfone)s with methoxy groups and spirobiindane groups (DMe-SBI) was synthesized from SBIBP ,DMHQ, and DFDPS in NMP with potassium carbonate by an aromatic nucleophilic condensation reaction.[8] The spiro-moieties were included for achieving a high gas permeability of the electrode binder.[11] The monomer equivalents of DMHQ: SBI/BP: DFDPS were 60:40:100 for polymerization of DMe-SBI, which was synthesized by a nucleophilic polycondensation reaction. As shown in Table. 3.1**,** DMe-BP had approximately 1.5 times higher molecular weights than those of DMe-SBI.

The demethylation reaction of DMe-SBI and DMe-BP using BBr_3 as the demethylation reagent was carried out in dichloromethane according to a previously reported method.[14] As a result of demethylation, the methoxy groups were 95% (DHy-SBI) and 84.0% (DHy-BP) converted to hydroxyl groups (Figure 3.2) After conversion of the polymer methoxy groups into hydroxyl groups, a chemical grafting process was carried out *via* the Williamson reaction to substitute the hydroxyl groups in the main-chain with bromoalkyloxy QA bromide.[8]

Table 3.1 Molecular weights of DMe-SBI and DMe-BP.

Ionomer	M_n (kg mol^{-1})	M_w (kg mol^{-1})	PDI
DMe-SBI	15.7	30.4	2.0
DMe-BP	22.9	96.2	4.2

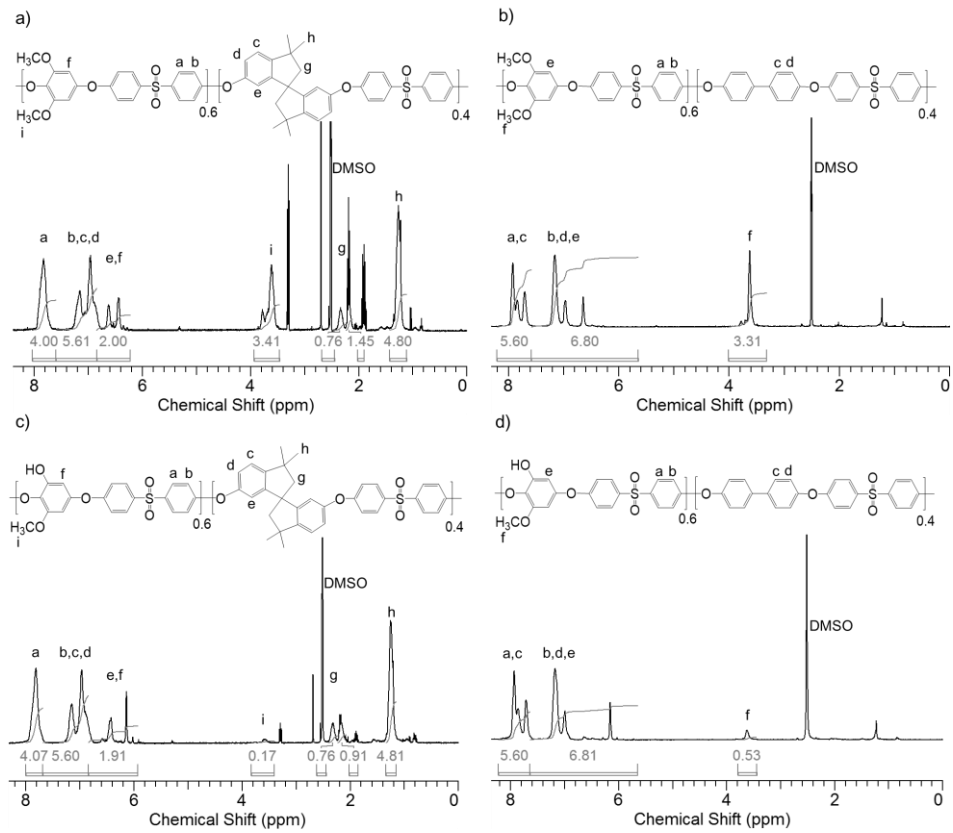

Figure 3.2 ^{1}H NMR spectra of a) DMe-SBI, b) DMe-BP, c) DHy-SBI, and d) DHy-BP.

(6-Bromohexyl)trimethylammonium bromide (Br-6-QA) was synthesized by the Menshutkin reaction of 1,6-dibromohexane with trimethylamine.[13] To prevent quaternization at both ends of the 1,6-dibromohexane, a dropping funnel was used. The ^{1}H NMR results indicated that Br-6-QA was obtained with a yield of 71.1%, about 2% of which di-quaternized byproducts. The peaks around 3.1 ppm are attributed to the $–CH_3$ of the QA groups, and the peaks around 3.3 ppm are attributed to the $–CH_2–$ near the QA groups. The peaks at 1.3, 1.4, 1.7, and 1.8 ppm are attributed to the chemical shifts of other $–CH_2–$ groups of the alkyloxy chain, and the peak of $–CH_2–$ near the Br groups appears at 3.5 ppm (Figure 3.3).

The D*n*-QBr-SBI and D*n*-QBr-BP copolymers were synthesized by Williamson reaction of Br-*n*-QA and DHy-SBI (or DHy-BP). Potassium carbonate and potassium iodide were used as the deacid reagent and catalyst in the reaction, respectively. The polymer structures were confirmed by ^{1}H NMR (Figure. 3.4). The DF_{NMR} values were measured from the peak area ratio of $–N^{+}–CH_3$ protons to aromatic protons in the ^{1}H NMR spectra and are listed in Table 2. The DF_{NMR} values of DHex-QBr-SBI and DHex-QBr-BP were close to the target values of 60 intended for polymerization. The DF_{NMR} values were then used to calculate IEC_{NMR} values, which were also similar to the $IEC_{Theoretical}$ values, confirming the synthesis. For comparison, DEth-QBr-SBI and DEth-QBr-BP were also prepared under the same reaction conditions. However, ethyloxy trimethylammonium side chains were hardly grafted onto DHy-SBI and DHy-BP, unlike the hexyloxy trimethylammonium side chains.

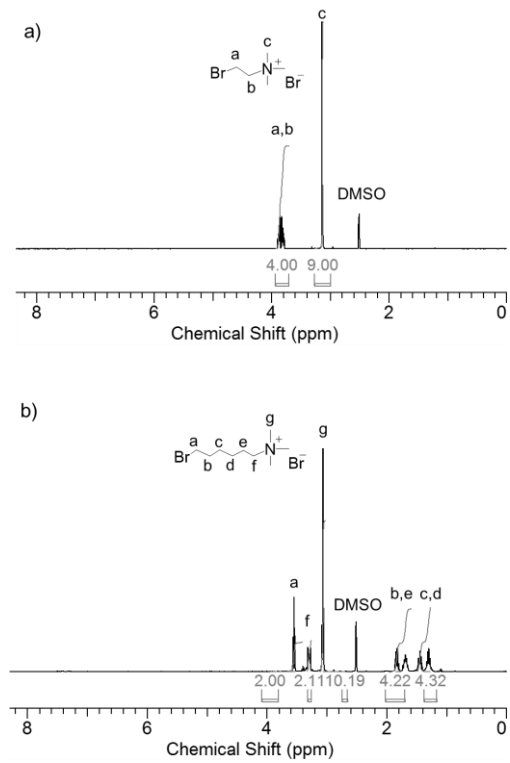

Figure 3.3 ^{1}H NMR spectra of a) (2-bromoethyl)trimethylammonium bromide (Br-2-QA) and b) (6-bromohexyl)trimethylammonium bromide (Br-6-QA).

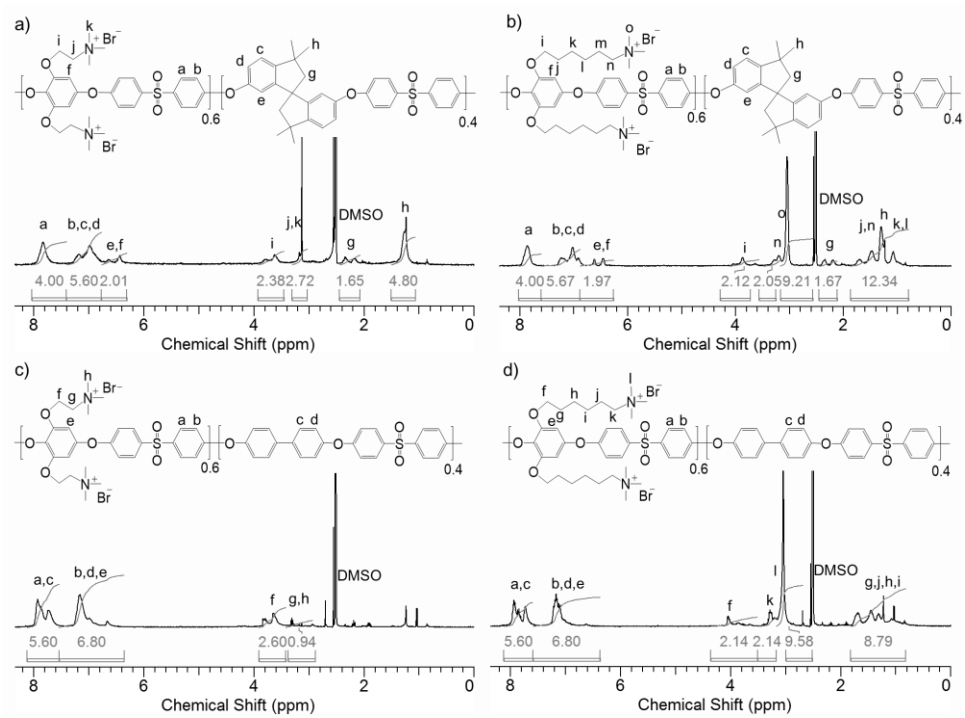

Figure 3.4 ^{1}H NMR spectra of a) DEth-QBr-SBI, b) DHex-QBr-SBI, c) DEth-QBr-BP, and d) DHex-QBr-BP.

As shown in Figure 3.4(a) and (c), the $–N^{+}–CH_3$ proton peaks of DEth-QBr-SBI and DEth-QBr-BP were very small in the ^{1}H NMR spectra. This seems to be due to a difference in reactivity between Br-6-QA and Br-2-QA, which is why the difference between the $IEC_{Theoretical}$ and IEC_{NMR} values of DEth-QBr-SBI and DEth-QBr-BP differ greatly (Table 3.2). In the previous report, there were no cases in which the ethyloxy trimethylammonium side chain was introduced.[8] Perhaps the synthesis was incomplete for the same reasons. All membranes were too brittle to measure other properties such as water uptake and conductivity.

The thermal stabilities of the ionomers were evaluated by TGA. As shown in Figure 3.5, all polymers had two thermal degradation steps. The first loss beginning at 180 °C could be due to the decomposition of alkyloxy trimethylammonium pendant groups, whereas the second loss beginning at 350 °C was attributed to the degradation of the polymer main chains. Thus, these ionomers have sufficient thermal stability at general operating temperatures of AEMFCs.

Table 3.2 Degrees of functionality and IEC values of DEth-QBr-SBI, DHex-QBr-SBI, DEth-QBr-BP, and DHex-QBr-BP.

Ionomer	DF_{Target} (QA %)	DF_{NMR} (QA %)	$IEC_{Theoretical}$ (meq g^{-1})	IEC_{NMR} (meq g^{-1})
DEth-QBr-SBI	60	15	1.93	0.55
DHex-QBr-SBI	60	51	1.74	1.54
DEth-QBr-BP	60	15	2.09	0.68
DHex-QBr-BP	60	53	1.87	1.73

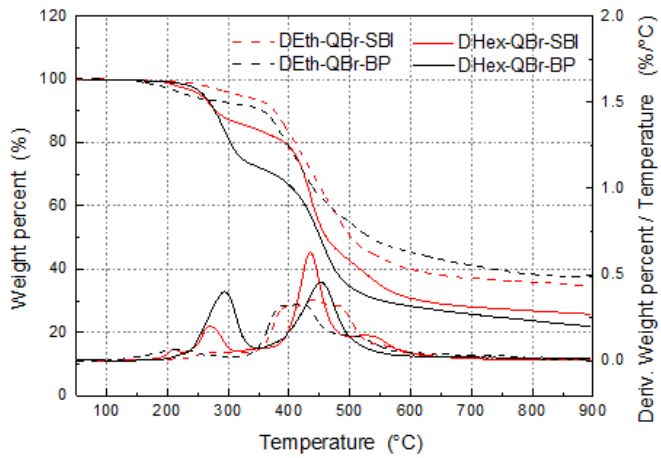

Figure 3.5 TGA results of DEth-QBr-SBI, DHex-QBr-SBI, DEth-QBr-BP, and DHex-QBr-BP.

DHex-QOH-SBI and DHex-QOH-BP were obtained by KOH treatment (1 M KOH solution at room temperature) of DHex-QBr-SBI and DHex-QBr-BP, respectively. As shown in Figure 3.6, the peak area ratio of the QA protons (3.03-3.31 ppm) to aromatic protons (6.27–8.03 ppm) decreased compared with the spectra in Figure 3.4. There was also an increase in the signals at 6.90-6.99 ppm and 7.72-7.74 ppm, which are marked with arrows, due to decomposition of the main-chain. The DF_{NMR} and IEC_{NMR} values were calculated from Figure 3.6 and are listed in Table 3.3. In comparison with the data in Table 3.2, the DF_{NMR} values of DHex-QOH-SBI and DHex-QOH-BP retained 86.3% and 84.9% of their values, respectively. Therefore, according to ^{1}H NMR, both polymers are unstable under strong alkaline conditions.

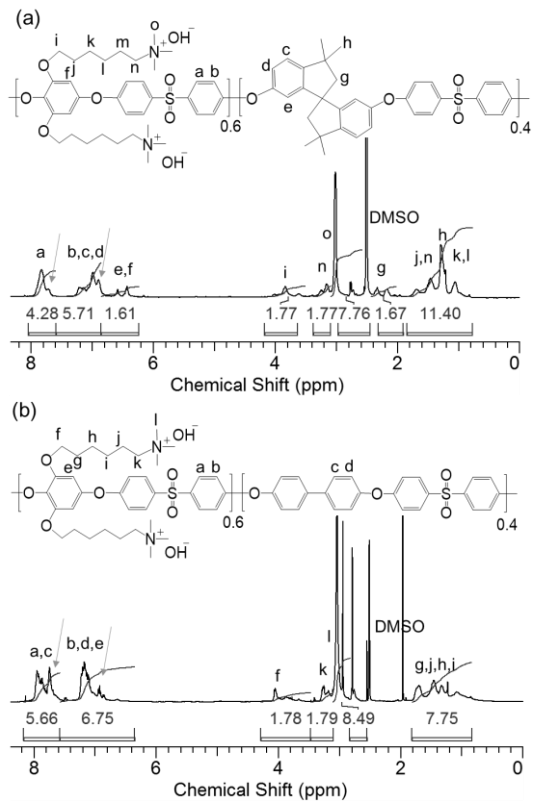

Figure 3.6 [1]H NMR spectra of a) DHex-QOH-SBI and b) DHex-QOH-BP.

Table 3.3 Degrees of functionality and IEC values of DHex-QOH-SBI and DHex-QOH-BP.

Ionomer	DF_{Target} (QA %)	DF_{NMR} (QA %)	$IEC_{Theoretical}$ (meq g^{-1})	IEC_{NMR} (meq g^{-1})
DHex-QOH-SBI	60	44	1.95	1.49
DHex-QOH-BP	60	45	2.12	1.72

3.3.2. Chemical stability of DHex-QOH-SBI

We investigated the effects on chemical stability of poly(arylene ether sulfone)s with QA hydroxide-functionalized side chains in alkaline environments. The alkaline stability tests of ionomers were performed by immersing the membranes in 0.1 M KOH at 60 °C for 170 h and 670 h. The samples were then washed and dissolved in DMSO-d_6 to obtain ^{1}H NMR spectra. The NMR results also showed a decrease in the peak area ratio of QA groups to aromatic protons. In addition, the integration ratio of the H_i and H_o peaks for DHex-QOH-SBI changed from 2.0:8.8 to 2.0:7.6, as expected for the partial decomposition of QA groups to trimethylamine or tertiary amine groups (Figure 3.7). In terms of the main-chain of the synthesized ionomers, a common pattern was observed at 6.90-6.99 ppm and 7.72-7.74 ppm.[15] It is known that nucleophilic attacks occur more easily on the *para*-position of the sulfone group.[16] and the degradation mechanisms of polymers in alkaline environment are known to be complicated processes.[5, 16, 17] Table 3.4 represent degrees of functionality and molecular weight of DHex-QBr-SBI and DHex-QOH-SBI after alkaline stability test. We confirmed that the analysis results on a polymer scale are consistent with those on a monomer scale.[18-20]

In an alkaline environment, QA groups are known to be degraded by nucleophilic substitution and β-hydrogen elimination (Figure 3.8). The length of the flexible spacer can have an influence on the alkaline stability of AEIs.[21] In the presence of two –CH_2– between the QA groups and electronegative ether

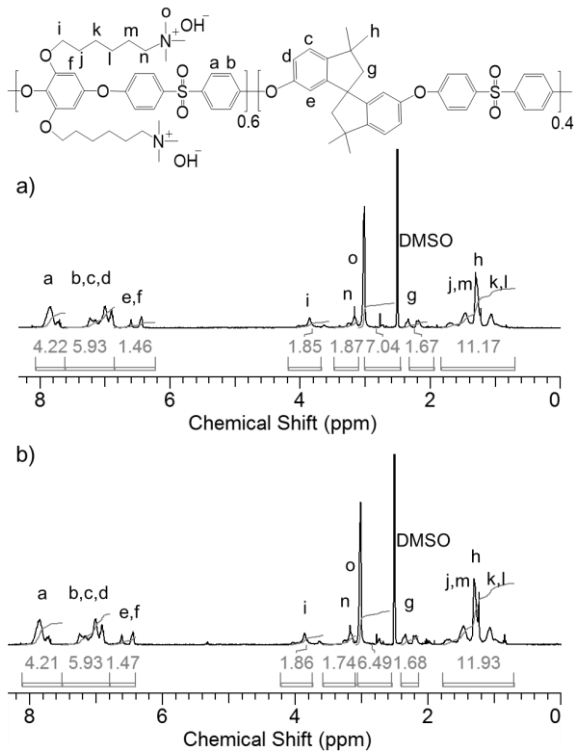

Figure 3.7 ^{1}H NMR spectra of DHex-QOH-SBI after alkaline treatment in 0.1 M KOH at 60 °C for a) 170 h and b) 670 h.

Table 3.4 Degrees of functionality and molecular weight of DHex-QBr-SBI and DHex-QOH-SBI after alkaline stability test.

Ionomer	DF_{NMR}	IEC_{NMR}	Molecular weight	
	(QA %)	(meq g^{-1})	M_n	PDI
DHex-QBr-SBI	51	1.74	8,797	1.15
DHex-QOH-SBI[a)]	47	1.58	6,207	1.41

[a)] After 0.1 M KOH treatment (168 h, 60 °C).

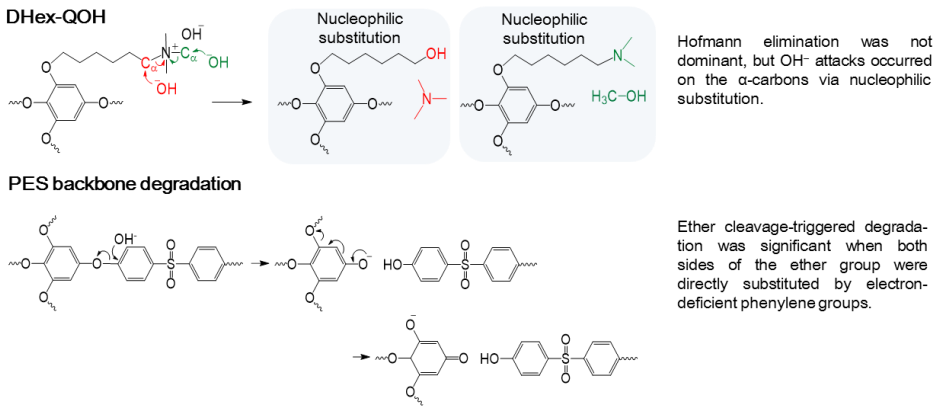

Figure 3.8 Alkaline degradation mechanism of DHex-QOH PES.

oxygen groups, the trimethylammonium groups seem to be degraded at the Williamson etherification stage, even in a relatively weak-base environment. The ethyloxy chain could thus not act as a spacer, which reduced the electron-withdrawing characteristics of the trimethylammonium groups and the reactivity of the β-hydrogen. It is known that the presence of the three –CH_2– between the QA and electronegative ether oxygen groups increases the reactivity of β-hydrogen, which is related to the Hofmann elimination reaction. When the alkyloxy side chain length is two or three, the C-O bond seems to be weaker than the C-C bond. In contrast, for alkylchain lengths of four or more, the alkaline stability of the C-O bond is similar that of the C-C bond.[8] The hexyloxy chain could make these β-hydrogen less acidic and inhibit the Hofmann reaction. Therefore, a long alkyloxy spacer could prevent the degradation of the trimethylammonium side chain.[22]

3.3.3. Single-cell performance of AEMFCs with DHex-QOH-SBI and DHex-QOH-BP as electrode binders

The single-cell test results confirmed that the synthesized ionomers can be used as electrode binders. Despite some chemical degradation in the alkali environment, both ionomers worked, as shown in Figure 3.9. We sprayed catalyst slurries using DHex-QOH-SBI and DHex-QOH-BP on the FAA-3-50 membrane. Single-cell performances of synthetic ionomers were the similar or lower level than other AEIs reported.24 Although it's about half the power density of the Fumatech FAA-3 binder and of a similar level, DHex-QOH-SBI showed a 1.2 times better single-cell performance than DHex-QOH-BP. A single-cell using DHex-QOH-SBI exhibited a

peak power density of 140 mW cm^{-2} and current density of 176 mA cm^{-2} at 0.6 V. Spiro-structure was proved to outstanding property for mass transport in electrode pore structure. This property was confirmed in polarization curves. Through these results, spiro-structure is considered to be suitable for AEIs due to the resulting relatively high gas permeable properties. This approach additionally allowed us to optimize cell performance by efficiently establishing the three-phase boundary without having problems such as water flooding caused by adjustment of the length/amount of side chains.

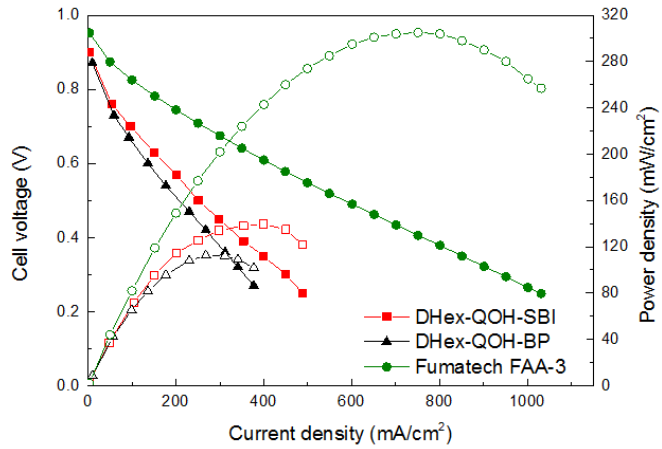

Figure 3.9 Single-cell performance results of AEMFC with DHex-QOH-SBI, DHex-QOH-BP, and Fumatech FAA-3 binders.

3.4. Conclusions

In this study, we investigated the effect of spirobiindane-based poly(arylene ether sulfone) ionomers with QA-functionalized alkyloxy side chains as AEMFC electrode binders. Poly(arylene ether sulfone)s with methoxy groups were prepared by nucleophilic substitution polycondensation. Then, the methoxy groups were demethylated to form hydroxyl groups for grafting QA-functionalized alkyloxy side chains. Unlike QA-functionalized hexyloxy side chains, ethyloxy side chains were hardly introduced onto DHy-SBI and DHy-BP. In the single-cell performance evaluation, DHex-QOH-SBI showed a 1.2 times higher maximum power density than DHex-QOH-BP. Instead of having problems caused by adjustment of the length/amount of side chains, the increased fractional free volume structure in the backbone allowed us to optimize cell performance by efficiently establishing the three-phase boundary. This investigation gives us considerable insight and direction for polymeric anion exchange ionomer designs.

3.5. References

[1] O.Z. Sharaf, M.F. Orhan, An overview of fuel cell technology: fundamentals and applications, *Renew. Sust. Energ. Rev.* (2014), **32**, 810-853.

[2] D.R. Dekel, Review of cell performance in anion exchange membrane fuel cells, *J. Power Sources* (2018), **375**, 158-169.

[3] H.-S. Dang, P. Jannasch, Alkali-stable and highly anion conducting poly (phenylene oxide)s carrying quaternary piperidinium cations, *J. Mater. Chem. A* (2016), **4**, 11924-11938.

[4] H.-S. Dang, P. Jannasch, Exploring different cationic alkyl side chain designs for enhanced alkaline stability and hydroxide ion conductivity of anion-exchange membranes, *Macromolecules* (2015), **48**, 5742-5751.

[5] L. Liu, X. Chu, J. Liao, Y. Huang, Y. Li, Z. Ge, M.A. Hickner, N. Li, Tuning the properties of poly(2,6-dimethyl-1,4-phenylene oxide) anion exchange membranes and their performance in H_2/O_2 fuel cells, *Energy Environ. Sci.* (2018), **11**, 435-446.

[6] H.-S. Dang, E.A. Weiber, P. Jannasch, Poly(phenylene oxide) functionalized with quaternary ammonium groups via flexible alkyl spacers for high-performance anion exchange membranes, *J. Mater. Chem. A* (2015), **3**, 5280-5284.

[7] L. Li, C.X. Lin, X.Q. Wang, Q. Yang, Q.G. Zhang, A.M. Zhu, Q.L. Liu, Highly conductive anion exchange membranes with long flexible multication spacer, *J.Membrane Sci.* (2018), **553**, 209-217.

[8] C.X. Lin, X.L. Huang, D. Guo, Q.G. Zhang, A.M. Zhu, M.L. Ye, Q.L. Liu, Side-chain-type anion exchange membranes bearing pendant quaternary ammonium groups via flexible spacers for fuel cells, *J. Mater. Chem. A* (2016), **4**, 13938-13948.

[9] S. Gottesfeld, D.R. Dekel, M. Page, C. Bae, Y. Yan, P. Zelenay, Y.S. Kim, Anion exchange membrane fuel cells: current status and remaining challenges, *J. Power Sources* (2018), **375**, 170-184.

[10] C.G. Arges, L. Zhang, Anion exchange membranes' evolution toward high hydroxide ion conductivity and alkaline resiliency, *ACS Appl. Energy Mater.* (2018), **1**, 2991-3012.

[11] J. Choi, M.-H. Kim, J.Y. Han, J.E. Chae, W.H. Lee, Y.M. Lee, S.Y. Lee, J.H. Jang, J.Y. Kim, D. Henkensmeier, S.J. Yoo, Y.-E. Sung, H.-J. Kim, Application of spirobiindane-based microporous poly(ether sulfone)s as polymeric binder on solid alkaline exchange membrane fuel cells, *J. Membrane Sci.* (2018), **568**, 67-75.

[12] F. Ishiwari, T. Sato, H. Yamazaki, J.N. Kondo, S. Miyanishi, T. Yamaguchi, T. Fukushima, An anion-conductive microporous membrane composed of a rigid ladder polymer with a spirobiindane backbone, *J. Mater. Chem. A* (2016), **4**, 17655-17659.

[13] A. C. Cope, R.D. Bach, trans-cyclooctene, *Org Synth* (1969), **49**, 39-43.

[14] Y. Kwon, S.Y. Lee, S. Hong, J.H. Jang, D. Henkensmeier, S.J. Yoo, H.-J. Kim, S.-H. Kim, Novel sulfonated poly(arylene ether sulfone) containing hydroxyl groups for enhanced proton exchange membrane properties, *Polym Chem.* (2015), **6**, 233-239.

[15] S. Miyanishi, T. Yamaguchi, Ether cleavage-triggered degradation of benzyl alkylammonium cations for polyethersulfone anion exchange membranes, *Phys. Chem. Chem. Phys.* (2016), **18**, 12009-12023.

[16] A.D. Mohanty, S.E. Tignor, J.A. Krause, Y.-K. Choe, C. Bae, Systematic alkaline stability study of polymer backbones for anion exchange membrane applications, *Macromolecules* (2016), **49**, 3361-3372.

[17] S.A. Nuñez, C. Capparelli, M.A. Hickner, N-alkyl interstitial spacers and terminal pendants influence the alkaline stability of tetraalkylammonium cations for anion exchange membrane fuel cells, *Chem. Mater.* (2016), **28**, 2589-2598.

[18] Z. Sun, B. Lin, F. Yan, Anion-exchange membranes for alkaline fuel-cell applications: the effects of cations, *ChemSusChem* (2018), **11**, 58-70.

[19] M.G. Marino, K.D. Kreuer, Alkaline stability of quaternary ammonium cations for alkaline fuel cell membranes and ionic liquids, *ChemSusChem* (2015), **8**, 513-523.

[20] J.B. Edson, C.S. Macomber, B.S. Pivovar, J.M. Boncella, Hydroxide based decomposition pathways of alkyltrimethylammonium cations, *J. Membrane Sci.* (2012), **399-400**, 49-59.

[21] A. Amel, S.B. Smedley. D. R. Dekel, M. A. Hickner, Y. Ein-Eli, Characterization and chemical stability of anion exchange membranes cross-linked with polar electron-donating linkers, *J. Electrochem. Soc.* (2015), **162**, F1047-F1055.

[22] Y. Chen, Synthesis and alkaline stability study of cationic perfluoroalkyl sulfonamide model compounds, in, Clemson University (2017), pp. 1-111.

국문초록 (Abstract in korean)

알칼라인 음이온 교환 막 연료전지 시스템은 비백금계 촉매(Ni, Mn, Co 등)를 쓸 수 있다는 장점이 있다. 산 환경에서보다 염기 환경에서 산소 환원 반응의 활성화 에너지가 낮아서 고가의 백금 촉매를 비백금계 촉매로 대체할 수 있는 여지가 더 크기 때문이다. 그럼에도 상용화 되기에 어려운 이유는 기존의 음이온 교환 막 연료전지용 전해질 막과 바인더 소재 중에서는 수소이온 교환 막 연료전지용의 것만큼 성능 및 내구성을 만족하는 소재가 없어서이다. 또한 대부분의 음이온 교환 막 연료전지 연구들은 전해질 막과 촉매에 대한 것들이었고 전극 바인더에 대한 연구는 매우 적다. 본 연구의 목적은 음이온 교환 막 연료전지용 기체 고투과성 전극 바인더를 개발하는 것이다.

1장에서는 연료전지를 이용한 전력 생산, 연료전지의 종류, 음이온 교환 막 연료전지용 고분자 전해질의 요건에 대하여 언급하였다.

2장에서는 스파이로바이인데인 그룹을 폴리아릴렌에테르설폰에 도입하여 내재적 미세 다공성 고분자 구조를 갖도록 한 내용을 다루었다. 음이온 교환 연료전지의 막 전극 접합체를 제조하는 데에 쓸 음이온 전도성 바인더 물질로 스파이로바이인데인과 사차암모늄 하이드록사이드 펜던트 그룹을 4중으로 갖는 신규 폴리아릴렌에테르설폰 고분자(QOH-SBI)를 합성하였다. 고분자의 기체 투과도를 확인하기 위하여 시간-지연

방법(time-lag method)이 사용되었다. 두꺼운 스파이로바이인데인과 얇은 아릴렌에테르설폰 단위가 서로 교차되는 사이에 고분자 체인 두께 차이가 있게 되고 이로 인해 생기는 분자수준에서의 미세 기공 때문에 기체 투과도가 높아지게 된다. 이는 광각 X선 회절(wide angle X-ray diffraction, WAXD) 결과로 고분자 체인 간 거리를 분석하여 스파이로바이인데인 그룹으로 인해 벌어지는 분자간 거리가 기체 투과 정도와 연관이 있음을 확인하였다. 또한 소각중성자산란(samll-angle neutron scatering, SANS) 결과로 고분자 체인의 구조 길이를 계산하였을 때에 스파이로바이인데인 구조로 인해 고분자 주쇄의 회전이 제한됨에 따라 경직도가 커진 점을 확인하였다.

높은 기체 투과 특성은 음이온 교환 막 연료전지 성능에 직접적으로 영향을 끼쳤다. 스파이로바이인데인이 있게 한 폴리아릴렌에테르설폰으로 만들어진 막 전극 접합체는 스파이로바이인데인이 없는 폴리아릴렌에테르설폰으로 만들어진 것보다 1.2배 높은 최대 파워 밀도를 보였고 특히 물질 전달 정도의 영향을 받는 고전류 밀도 영역에서 높은 성능을 보였다. QOH60-SBI40을 이용하여 제조한 MEA는 223 mW cm^{-2}의 최대 파워 밀도, 0.6 V에서 280 mA cm^{-2}의 전류 밀도의 성능을 나타냈다.

3장에서는 알칼라인 음이온 교환 막 연료전지 전극 바인더 물질로 사차 암모늄 작용 그룹이 있는 알킬옥시 측쇄를 갖는 폴리아릴렌에테르설폰 고분자를 합성한 내용을 나타냈다. 주쇄와 측쇄를 다르게 하여

전극 바인더 고분자들을 합성하였고 합성한 고분자들은 핵자기공명(NMR) 분광법, 열중량분석법을 통해 분석하였다. 이 고분자를 사용한 단위 전지 성능 시험도 행해졌다. 사차 암모늄 작용 그룹이 있는 헥실옥시 측쇄를 갖는 스파이로바이인데인 기반 폴리아릴렌에테르설폰 고분자는 음이온 교환 막 연료전지 적용에 있어 가능성을 보였다. 이 고분자를 사용한 MEA는 140 mW cm^{-2}의 최대 파워 밀도를 나타냈으며 이는 주쇄에 바이페닐이 있는 것보다 1.2배 높은 값이었다.

이 접근 방법은 음이온 교환 막 연료전지 성능을 최적화하기 위하여 기존의 이온성 측쇄의 길이나 양의 조절하는 방법으로 인해 발생되는 문제를 피하면서도 20% 정도의 최대 파워 밀도를 부가적으로 증가시킬 수 있게 한다는 이점이 있다.

주요어: 음이온 교환 막 연료전지, 바인더, 고분자 전해질, 내재적 미세 다공성 구조, 폴리아릴렌에테르설폰, 스파이로바이인데인

학 번: 2014-30257

List of publications (SCI)

1st or co-1st author

Jieun Choi, Man-Ho Kim, Jun Young Han, Ji Eon Chae, Won Hee Lee, Young Moo Lee, So Young Lee, Jong Hyun Jang, Jin Young Kim, Dirk Henkensmeier, Sung Jong Yoo, Yung-Eun Sung and Hyoung-Juhn Kim, Application of spirobiindane-based microporous poly(ether sulfone)s as polymeric binder on solid alkaline exchange membrane fuel cells, *J. Membrane Sci.* (2018), **568**, 67-75.

Jieun Choi, Young-Jun Byun, So Young Lee, Jong Hyun Jang, Dirk Henkensmeier, Sung Jong Yoo, Seong-Ahn Hong, Hyoung-Juhn Kim, Yung-Eun Sung and Jin-Soo Park, Poly(arylene ether sulfone) with tetra(quaternary ammonium) moiety in the polymer repeating unit for application in solid alkaline exchange membrane fuel cells, *Int. J. Hydrogen Energy* (2014), **39**, 21223-21230.

Jieun Choi, Jue-Hyuk Jang, Ji Eon Chae, Hee-Young Park, So Young Lee, Jong Hyun Jang, Jin Young Kim, Dirk Henkensmeier, Sung Jong Yoo, Kwan Young Lee, Yung-Eun Sung and Hyoung-Juhn Kim, Spirobiindane-based poly(arylene ether sulfone) ionomers for alkaline anion exchange membrane fuel cells, *In Press, Accepted to Macromol. Res.* (2019).

Co-author

Hye-Jin Lee, Yeonhye Kwon, So Young Lee, Jieun Choi, Bo Hyun Kim, Dirk Henkensmeier, Jong Hyun Jang, Sung Jong Yoo, Jin-Young Kim, Hyoung-Juhn Kim, Hwayong Kim and Man-Ho Kim, Facile preparation of a long-term durable nano- and micro-structured polymer blend membrane for a proton exchange membrane fuel cell, *RSC Adv.* (2016), **6**, 46516-46522.

Ju Yeon Lee, Dong-Hee Lim, Ji Eon Chae, Jieun Choi, Bo Hyun Kim, So Young Lee, Chang Won Yoon, Sang Yong Nam, Jong Hyun Jang, Dirk Henkensmeier, Sung Jong Yoo, Jin-Young Kim, Hyoung-Juhn Kim and Hyung Chul Ham, Base tolerant polybenzimidazolium hydroxide membranes for solid alkaline-exchange membrane fuel cells, *J. Membrane Sci*. (2016), **514**, 398-406.

Hye-Jin Lee, Jieun Choi, Jun Young Han, Yung-Eun Sung, Dirk Henkensmeier, Eun Ae Cho, Jong Hyun Jang, Sung Jong Yoo, Hyoung-Juhn Kim and Hwayong Kim, Synthesis and characterization of poly(benzimidazolium) membranes for anion exchange membrane fuel cells, *Polym. Bull.* (2013), **70**, 2619–2631.

Dongwon Shin, Adam Febriyanto Nugraha, Farid Wijaya, Sojeong Lee, Eunyoung Kim, Jieun Choi, Hyoung-Juhn Kim and Byungchan Bae, A novel synthetic method for advanced multi-block anion exchange membrane applications, *RSC Adv.* (2019), **9**, 21106-21115.